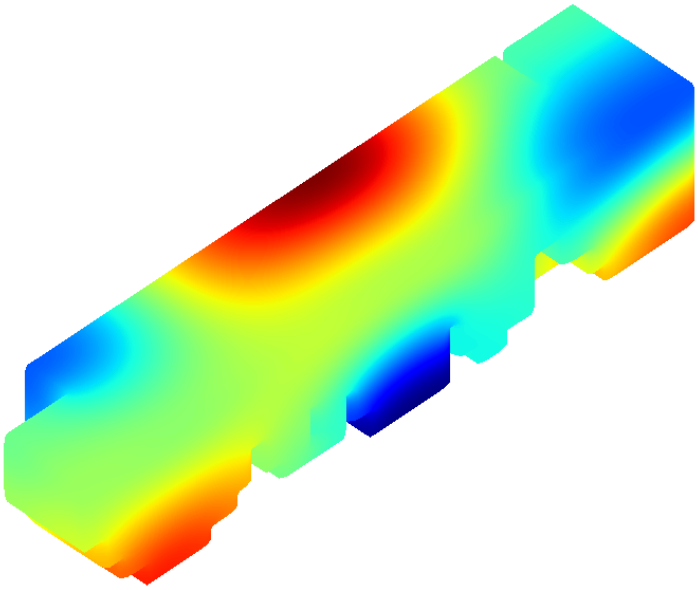

Impact of Cavity Modes on the Acoustic Environment of a Bus Cabin

Investigation to find an appropriate way to predict the modes of a bus cabin by three different methods: sound pressure measurements, frequency response measurements and FEM simulation

Master's thesis in Master Programme Sound and Vibration

LUCÍA GONZÁLEZ GONZÁLEZ
KAJSA MAGNUSSON

Department of Architecture and Civil Engineering, Division of Applied Acoustics
CHALMERS UNIVERSITY OF TECHNOLOGY
Göteborg, Sweden 2022
www.chalmers.se

Master's thesis 2022

Impact of Cavity Modes on the Acoustic Environment of a Bus Cabin

Investigation to find an appropriate way to predict the modes of a bus cabin by three different methods: sound pressure measurements, frequency response measurements and FEM simulation

Lucía González González & Kajsa Magnusson

CHALMERS
UNIVERSITY OF TECHNOLOGY

Department of Architecture and Civil Engineering
Division of Applied Acoustics
Chalmers University of Technology
Göteborg, Sweden 2022

Impact of Cavity Modes on the Acoustic Environment of a Bus Cabin

Investigation to find an appropriate way to predict the modes of a bus cabin by three different methods: sound pressure measurements, frequency response measurements and FEM simulation

LUCÍA GONZÁLEZ GONZÁLEZ
KAJSA MAGNUSSON

Supervisor: Conrado de Mello Calvet, Volvo Buses
Examiner: Wolfgang Kropp, Department of Architecture and Civil Engineering

Master's Thesis 2022
Department of Architecture and Civil Engineering
Division of Applied Acoustics
Chalmers University of Technology
SE-412 96 Göteborg
Telephone +46 31 772 1000

Cover: Tenth acoustic mode corresponding to 74.4 Hz of the cabin of the bus.

Typeset in LaTeX
Printed by Chalmers Reproservice
Göteborg, Sweden 2022

Impact of Cavity Modes on the Acoustic Environment of a Bus Cabin
LUCÍA GONZÁLEZ GONZÁLEZ & KAJSA MAGNUSSON
Department of Architecture and Civil Engineering
Chalmers University of Technology

Abstract

The minimization of noise exposure for passengers and drivers inside a bus is important to improve their comfort as well as to enhance the product image. The acoustic modal response of the bus cavity has a major effect on the noise levels perceived by users. Three different methods were performed in this thesis to find the main modes in the bus cavity: FEM simulation of a simplified model, Sound Pressure Level measurements under operation and FRF measurements. The resonant frequencies obtained with each method were compared in order to identify possible noise sources amplifying these modes. The frequency range that is thoroughly analyzed in this report is between 0 Hz and 100 Hz as it includes the lowest modes, which are more likely to affect the perception of the sound environment in the cabin. The results show a clear correlation in frequency between the different methods, making it possible to separate modes excited by the cavity, by the structure of the bus or by other noise sources, especially at low frequencies. However, the results from the different methods do not correlate as good above 70 Hz. Possible reasons for this could be the increased modal density or the damping in the cabin that is not simulated in the model. On this basis, it can be concluded that the use of both simulation and experimental measurements to obtain FRFs in the cavity of a bus cabin up to 70 Hz is beneficial to understand the acoustic behaviour of the bus.

Keywords: acoustical excitation, bus, FEM, frequency response function, FRF, modal analysis, resonance.

Acknowledgements

First of all, we would like to pay our special regards to Conrado de Mello Calvet who has been a great supervisor throughout the thesis work. He has always been available for all our big and small questions, guiding us through the Volvo jungle with endless patience and support. Also for being the one introducing us to Franky Boy, who became our trustworthy companion. This thesis would not have been possible without Conrado as well as Birgitta Andersson, who initiated the project, and for that, we are forever grateful.

We should also appreciate the discussions we have had with Professor Wolfgang Kropp, who was very enlightening and gave us direction when we felt lost. We would also like to thank Markus Andmarsjö, David Lantz and Anders Hedlund for their help in areas of expertise.

We also want to express our gratitude to Martín Sandoval and all our colleagues at Volvo Buses that have made us feel welcome and a part of the team during this time. They have all been helpful and supportive, even during times when we exchanged the radio hits for white noise in the workshop. We would like to especially thank Tania Stamatina for the unconditional cheering, laughs, wise words, and detailed proofreading of the report, as well as the tea.

Lastly, we thank Volvo Buses for the facilities and the opportunity to work in this environment. The possibility to involve a lot of practical elements in the thesis work was very instructive and we will bring this knowledge with us for a very long time. Our measurements would not have been possible without the help from our colleagues at Group Trucks Technology, who contributed with experience and equipment. The help we got from the FFT support and especially Maira Cortese was invaluable and led to the good impression we now have of *Actran*.

I want to thank my parents and sisters, my partner in crime Lucas, and the rest of my family. Gracias por vuestro apoyo incondicional durante estos dos años y en cada decisión que tomo. ¡Os quiero!

Lucía González González

I am very grateful for all the support and encouragement I have gotten from my friends and especially my family during my years at Chalmers. Thank you for everything!

Kajsa Magnusson

Göteborg, June 2022

List of Acronyms

Below is the list of acronyms that have been used throughout this thesis listed in alphabetical order:

1D, 2D, 3D	One, Two and Three Dimensional
BEM	Boundary Element Method
CAD	Computer Aided Design
DFR	Direct Frequency Response
FEM	Finite Element Method
FFT	Fast Fourier Transforms
FRF	Frequency Response Function
IR	Impulse response
MLS	Maximum Length Sequence
RPM	Revolutions Per Minute
SEA	Statistical Energy Analysis
SNR	Signal-to-Noise Ratio
SPL	Sound Pressure Level
WOT	Wide Open Throttle

Contents

1

Introduction

This thesis was conducted in collaboration with Volvo Buses to investigate the impact of the modes in a bus cabin cavity. Both Finite Element Method simulations and Frequency Response measurements, as well as Sound Pressure Level measurements, were performed to identify the main noise sources and problematic frequencies. The main objective is to compare both simulations and measurements in order to conclude whether the proposed simulations are a good tool to define the critical points and frequencies inside the bus, and therefore help the company to further develop its products in the most efficient way possible.

1.1 Background

The identification of noise sources in products or environments dates back to ancient times. Nevertheless, it was not until recent decades when the acoustic of interior environments such as rooms, industries or passenger vehicles became an important area of study, as the annoyance of these sources started to be considered a health-related issue. According to The World Health Organization, regular exposure to high sound levels can cause stress, sleep disturbance, cardiovascular effects, hypertension or hearing loss, as well as an inadequate performance of tasks due to insufficient concentration, interfering therefore in the daily activities of the population [1]. Because of this, and focusing now on the automotive industry, it is important to design and develop vehicles to minimize this noise exposure to the passengers. This helps not only to improve the health-related conditions of the drivers and regular users but also to increase customer satisfaction and comfort. It also enhances the product image, as a quiet environment and low interior noise usually define the high quality vehicles.

To minimize the interior noise in a bus, the typical noise control approach is to reduce the overall noise level in the cabin and to keep the sound quality parameters such as Reverberation Time, Early Decay Time or Transmission Index within the desired levels. This approach can lead to an important increase in cost due to the treatment of all sources, especially in a product with such large dimensions as a bus. However, the modal response of the interior of the bus can also have a major impact on the comfort of the passengers due to the distribution of the sound pressure, resulting in areas with high noise levels. Therefore, the identification of the acoustic modes, their frequencies and the critical positions within the bus cabin can lead, not only to an improvement in passenger comfort, but also to a reduction in the overall

cost of the noise mitigation treatments.

The Impulse Response or Frequency Response measurement is a very good descriptor to understand the modal behaviour of the cabin of the bus. If a good measurement procedure is defined it is easy to identify the first acoustic resonances taking into account all specific features or materials inside the cabin, as well as to calculate other acoustic parameters if needed. However, it is useful to be able to predict and adjust the acoustic behaviour of the bus in the design stage, before the manufacturing of the product. This would help to reduce time, effort and costs at a later stage of the development process, where large amounts of absorptive material would be needed to control the acoustics of the bus, especially at low frequencies.

FEM is a good numerical approach for the modelling of the bus and the prediction of interior noise levels at low frequencies. The use of this method in acoustics was initiated in 1965 by Gladwell [2] and since then, it has been widely applied in various fields, the automotive sector among others, as presented in [3], [4] or [5]. However, it is usually used for modelling small cavities such as cars, but its use is not as popular for larger vehicles such as buses. Therefore, that is the scope of study of this thesis.

1.2 Aims

The aims of this thesis work are summarized as follows:

- To create an adequate and simple model of the cavity of a bus and to perform an acoustic modal analysis by FEM simulation.
- To perform Sound Pressure Level (SPL) measurements of the bus under operation.
- To develop an acoustic Frequency Response Function (FRF) measurement procedure and perform measurements in the cabin.
- To compare the resonances obtained with the three methods.

1.3 Description of the Bus Under Test

The bus under test is a Volvo 7900 Electric Hybrid, a city bus with two axles and a rear driveline, equipped with a four-cylinder diesel engine D5K 240 [6], an electric motor and an I-Shift gearbox AT2412E [7] with 12 forward gears and 4 reverse gears. Sound absorbers made of glass wool and covered in thermoplastic polyvinylidene fluoride (PVDF) are installed in the engine compartment [8].

The overall exterior measures are 12.1 m long, 2.5 m width and 3.3 m height, and the inner dimensions are 11.8 m long, 2.4 m width and 2.6 m height. It has 30 passenger seats covered with upholstery fabric. A picture of the bus can be seen in Figure 1.1.

Figure 1.1: General overview of bus Volvo 7900 Electric Hybrid. Picture from [8].

1.4 Outline of the Thesis

In this section, the structure of this thesis is described. It consists of five chapters which are summarized below.

First, in the *Introduction*, some background information on the topic of study as well as the goals of this project are presented to provide the reader with a general idea and to understand the motivation for this thesis.

Secondly, the *Theory* chapter serves as a guide with the fundamental concepts to gain an understanding of the work presented throughout the thesis. It includes the necessary knowledge about modal analysis and the different measurements performed and justifies the selected method for each of them.

Moreover, the *Methods* chapter, which is divided in simulation, SPL measurements and FRF measurements, includes an explanation of the used method, as well as a detailed description of the measurement procedures, setup and equipment used to perform the tests.

In the *Results and Discussion* chapter, all results are shown followed by a discussion of the findings. This chapter is also divided into the same sections as the method: simulation, SPL measurements and FRF measurements; but it includes also a section comparing the resonances found with the different methods.

Lastly, the *Conclusion* summarises the major findings from the work performed and from the comparison between the different methods to obtain the modes in the bus.

2

Theory

In this chapter, the fundamentals of the theory of modal analysis and FEM are described in order to have a better understanding of the main concepts described and analysed later in this report. The reason why the SPL measurements are of importance to identify critical points in the bus, as well the acoustic frequency response and the different methods to calculate it and represent it, are also described.

2.1 Frequency Range of Interest

The frequency range that will be taken into account in this report is from 0 Hz to 200 Hz. One reason for this is that many mechanisms in a vehicle, such as engine and compressor, can potentially excite the cavity in this range and, in extent, have a great impact on the passengers. Another major limiting factor is the modal density, which increases with frequency. The dimensions of the bus are strongly connected to the modal density and it would be difficult to identify the separate modes if higher frequencies were included. One benefit of this selected range is that analytical and simulated results can easily be performed with simple methods at a low frequency; this will be further discussed later on in this report.

2.2 Modes of a Rectangular Box

The modes of a rectangular box or room are of importance because they can amplify unwanted noises at certain frequencies. The modes occur when a standing wave arises in the cavity and cause high pressure amplitudes. If modes in a bus cabin are excited they might annoy the passengers at certain seats. Standing waves can appear in multiple directions at the same time and they depend on the dimension of the room. The equations in this section are to be found by Vigran [9]. The frequency of the mode is described by

$$f = \frac{c}{2}\sqrt{\left(\frac{n_x}{L}\right)^2 + \left(\frac{n_y}{W}\right)^2 + \left(\frac{n_z}{H}\right)^2} \tag{2.1}$$

where n_x, n_y, n_z are the orders of the mode in the different directions, c is the speed of sound and L, W and H are the length, width and height of the room respectively. This is the analytical initial calculation to be compared with the measured data since the bus is close to a rectangular room in its dimensions.

The eigenfunction, i.e. sound pressure at different points (x, y, z) in the room, can be calculated as

$$p(x, y, z) = A \cdot \cos\left(\frac{n_x \pi x}{L}\right) \cdot \cos\left(\frac{n_y \pi y}{W}\right) \cdot \cos\left(\frac{n_z \pi z}{H}\right) \tag{2.2}$$

where A is the pressure peak value and the other variables are the same as in equation 2.1.

Figure 2.1 shows the three different types of modes that can occur in a hexahedral room. Their pressure distribution is calculated with Equation 2.2. The modes can be axial (only in one direction), tangential (modes in two directions) and oblique (modes in all three dimensions). The first modes will be axial in the length direction of the bus, because it is much longer than high and wide, and they are usually the most dominant ones.

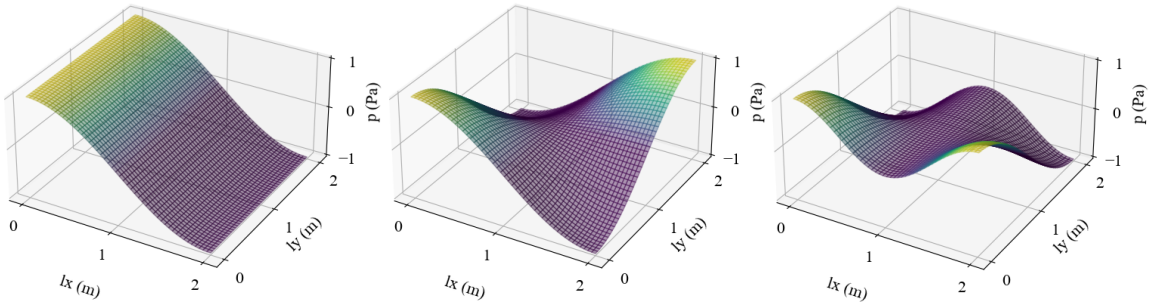

(a) Axial Mode (1,0,0) **(b)** Tangential Mode (1,1,0) **(c)** Oblique Mode (1,1,1)

Figure 2.1: Different mode types in a box.

The number of modes, N, that possibly can occur below a certain frequency, f, is calculated by

$$N = \frac{4\pi V}{3c^3} f^3 + \frac{\pi S}{4c^2} f^2 + \frac{L}{8c} f \tag{2.3}$$

where V is the volume of the cavity,

$$V = l_x l_y l_z. \tag{2.4}$$

S is the surface area calculated as

$$S = 2(l_x l_y + l_x l_z + l_y l_z) \tag{2.5}$$

where l_x, l_y and l_z is the length between the corners in the room. Finally, L is is the total corner length given as

$$L = 4(l_x + l_y + l_z). \tag{2.6}$$

The coordinate system that will be used throughout the report is shown in Figure 2.2, and follows the standard for vehicles with the origin in the corner where the driver is located. The modal numbers are defined as (x, y, z).

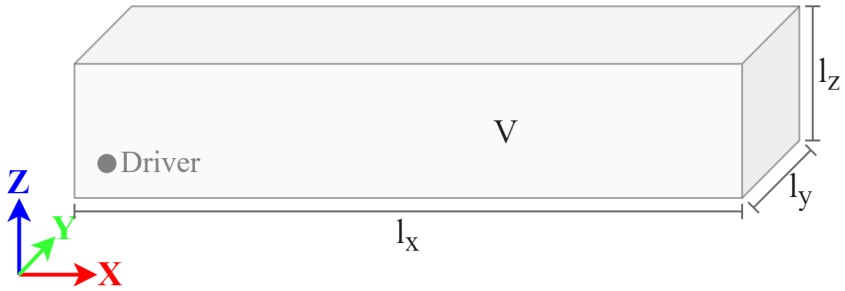

Figure 2.2: The coordinate system used to describe positions and directions in the bus.

2.3 Finite Element Method

There are many different engineering methods to solve numerical problems within acoustics. All of them differ when it comes to computational cost and how easy a model can be set up, as well as accessibility to commercial software. Two common high frequency methods are SEA and geometrical acoustics. However, only the low frequencies are of interest and these methods will therefore not be further discussed. The most common low frequency techniques are FEM and BEM. According to [10], BEM can not compete with FEM when it comes to solving interior acoustic problems. This is because FEM enables volume discretization, compared to BEM, which has an advantage when the boundaries are more complex. The desire to calculate the pressure distribution in a simple model with rigid boundaries makes FEM a preferable choice for the simulations in this thesis.

The Finite Element Method is a widely used method to solve differential equations numerically. The model to be analysed is divided into finite elements to facilitate the solving process resulting in an approximate solution. The method is applied in many engineering topics, especially mechanics, as well as acoustics. The fundamentals in acoustics and how FEM is applied on this topic are well documented [11] and will not be described into further detail in this report. The mathematics and solver procedure are explained in detail in the User Guide for *Actran* [12], which is the software used.

The mesh is of importance to get a level of certainty in the simulation results. For acoustic simulations, the number of elements per wavelength is the most common criterion to evaluate the mesh quality. The amount of elements per wavelength is dependent on the analysis to be performed as well as on the element types used and it is a widely discussed topic [13]. In [14] it is recommended to use more than the thumb rule of six elements for linear elements, which is used in this study. Therefore, the choice was made to use eight elements per wavelength, to reduce the error of the calculated sound pressure and at the same time not increase the computational cost unnecessarily.

The size of the elements is directly dependent on the frequency range of interest and the chosen amount of elements per wavelength (in this case eight). The maximum element size should be

$$h_{max} = \frac{\lambda_{min}}{8} \tag{2.7}$$

based on the minimum wavelength λ_{min}, i.e. maximum frequency of interest. With an upper frequency limit of 200 Hz and eight elements per wavelength, the longest element size should be 1.7 m.

2.4 Sound Pressure Level in a Bus Cabin

An essential tool to understand the behaviour of the bus under real conditions, and therefore investigate at which noise levels are the driver and passengers exposed, is to conduct SPL measurements under operation. These measurements can be performed while driving at different modes and speeds to observe how the different conditions influence the sound levels in the cabin. By obtaining these levels at various positions in the bus, it is possible to know the most dominant noise sources and the frequencies that are normally excited during the operation, as well as to identify critical locations in the cabin that may cause noise annoyance to the driver or passengers.

Considering that the bus is the workplace for the drivers and they may spend up to eight hours exposed to the same noise sources, it is even more important to minimize the exposure to high sound levels. According to ISO-16121-4 [15], the equivalent continuous A-weighted SPL over time, L_{AeqT}, at the driver position shall not exceed 70 dBA at 50 km/h and 60 dBA at stationary conditions when the engine is idling. There are no specific requirements for the rest of the bus, but the goal should be to maintain the sound levels as low as possible.

2.5 Acoustic Frequency Response

The Impulse Response (IR), $h(t)$, and its corresponding Acoustic Frequency Response Function (FRF), $H(f)$, are fundamental concepts to observe the behaviour of a room or a bus cabin, assuming they are linear systems. The most common approach to obtain these results is in the time domain, calculating the IR by exciting the room with a known signal. For this purpose, some methods that use different excitation signals have been studied, with the most common ones MLS, inverse repeated sequence, time-stretched pulses and sine sweep signals [16]. Although they can be efficient methods depending on the measurement case and frequency range of interest, the main disadvantages are the influence of the nonlinearities of the source in the results or the lengthy calibration needed to eliminate this impact [17]. Another limiting factor is the frequency response of the loudspeaker, which makes it difficult to obtain good results at relatively low frequencies. In this thesis, the main focus is on the frequency response of the cabin, especially at low frequencies, as the

first natural frequencies of the cavity under test are of interest, and the described methods are not optimal for this.

To achieve better results at the desired frequency range and to avoid the distortions caused by usual noise sources, a low-frequency volume acceleration source (Q-source) can be used [18]. The output of this source is a volume displacement signal in $\mathrm{Pa/m^3}$, so a double integration of it needs to be done to obtain volume acceleration, Q, before the calculation of the FRF. Then, $H(f)$ can be calculated directly in the frequency domain as

$$H(f) = \frac{Y(f)}{X(f)} = \frac{p}{Q}\ \frac{\mathrm{Pa}}{\mathrm{m^3/s^2}} \tag{2.8}$$

where the output $Y(f)$ is the sound pressure of the microphones, p, and the input $X(f)$ is the volume acceleration of the source, Q.

However, using the input and output spectra to calculate the FRF does not provide optimal results due to the instrumentation noise introduced mainly by the microphones (output). Consequently, it produces variation in the results between different measurements leading therefore to uncertain results. A more appropriate technique to calculate the FRF and obtain reliable results assuming minimal noise at the input is the H1-estimator, which is calculated as

$$H_1(f) = \frac{S_{yx}(f)}{S_{xx}(f)} \tag{2.9}$$

where $S_{xx}(f)$ is the auto-spectrum of the input signal and $S_{yx}(f)$ is the cross-spectrum of the system, which determines the relationship between both signals:

$$S_{xx}(f) = X(f) \cdot \overline{X(f)} \tag{2.10}$$

$$S_{yx}(f) = Y(f) \cdot \overline{X(f)}. \tag{2.11}$$

In addition, there is a parameter to observe the relationship between input and output of the system and thus, the reliability of the measurements: the coherence $\gamma^2_{xy}(f)$, calculated as

$$\gamma^2_{xy}(f) = \frac{\mid S_{yx}(f) \mid^2}{S_{xx}(f) \cdot S_{yy}(f)}, \tag{2.12}$$

where $S_{yy}(f)$ is the auto-spectrum of the output signal, calculated as that of the input and $0 \leq \gamma^2_{xy}(f) \leq 1$. Values of the coherence close to 1 are a good indicator of reliability as they indicate consistency between measurements, while values close to 0 can indicate an error in the measurement setup or a bad Signal-to-noise ratio (SNR), which could be due to background noise in the measurement site or insufficient excitation by the source.

FRF is a complex function and is commonly expressed in magnitude/phase or imaginary/real parts. The two of them are shown in Figure 2.3 taking one microphone and source position in the bus under test as an example. On one hand, the magnitude curve shows all resonances as positive peaks and the phase change can be observed around the resonant frequencies. On the other hand, while the imaginary part of the FRF has clear peaks and dips at the resonance frequencies, the real part is zero at these frequencies, which makes the identification of them more complicated. Additionally, by looking at the imaginary part of each microphone position separately it would be possible to obtain information about the mode shapes; but more microphone positions would be necessary for this purpose and it is not included in the scope of this thesis.

Because of the described above, both the imaginary part of the FRF and the magnitude in dB would be good representations of the FRF. However, when plotting several positions at the same time, the widest peaks, which correspond to the modes with high damping, are more difficult to identify precisely. Additionally, the peaks that are very close to each other are also hard to separate, as can be observed in Figure H.4 and Figure H.5 (Appendix H), where the results from the FRF with the source 4 as the excitation are represented in imaginary part and magnitude respectively. Consequentially, the imaginary part of the FRF was selected as the optimal way to identify the acoustic modes in the bus and it is, therefore, the representation used in all figures at Section 3.3 and Section 4.3.

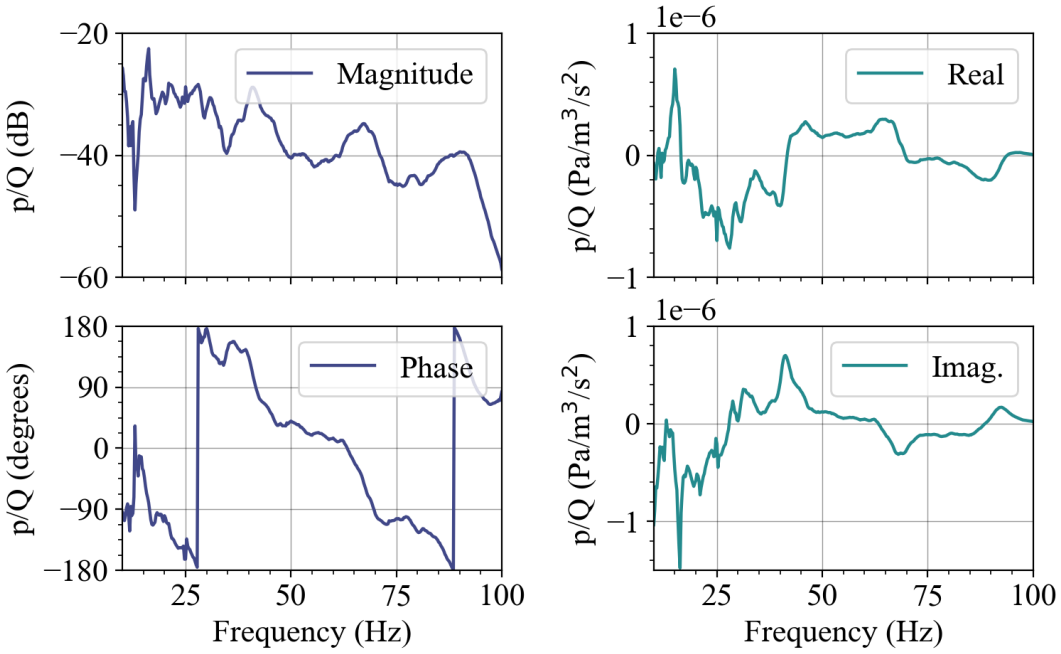

Figure 2.3: Magnitude and phase plots (left) and real and imaginary parts (right) of the FRF.

3

Methods

The chosen numerical method to estimate the sound pressure levels in the bus cavity was FEM. The setup in the software and mesh criteria for the different models is further described in this chapter. Both SPL in operation and FRF measurements have been performed in the bus and the methodological description, setup and measurement conditions are also described in this chapter. In Appendix A a detailed list of all used equipment to perform both measurements is shown, as well as a diagram showing the FRF measurement chain. Appendix B contains pictures of the setup of all microphones, accelerometers and source positions.

3.1 Simulation

The software used for the acoustic FEM simulation was *Actran 2021* from *MSC Software*. Two different models were made: one simple rectangular box and one more similar to the actual bus. The latter model was also used to simulate the frequency response at the microphone positions with the activated sources. How the models and analyses were defined is explained in the following sections but extensive information about the setup and calculation of the analyses in *Actran* can be found in *Actran 2021 User Guide Vol. 1* [12].

3.1.1 Modes of a Rectangular Box

Firstly, the number of modes and the eigenfrequencies of a rectangular box were simulated. The modes were calculated analytically to have a preliminary idea of the expected acoustic modes in the frequency range 0 Hz to 200 Hz, where the acoustic response is expected to be more problematic as the modal distribution is irregular in space and frequency. Afterwards, the microphone positions for the experiments could be chosen based on the pressure distribution, as well as the sources, so that they would excite the modes efficiently. The need for a more advanced FEM model for future work can also be discussed based on the difference between this simple analytical model compared to the bus model presented in Section 3.1.2.

The analysis performed for the modes was a modal extraction. The rectangular box had the interior dimensions of the bus under test: 11.80 m x 2.41 m x 2.57 m. The mesh was made coarse because the first 20 modes, which will be compared in detail and are of high importance, are below 100 Hz. The chosen mesh did not have any element larger than 0.425 m; which was the largest element size allowed in this

study, as described in Section 3.1.2. The model consisted of 8407 nodes and 43702 elements and the boundaries were considered rigid.

3.1.2 Bus Model

A simplified model of the bus was also created in *Actran* to perform an analysis of the modal response and the frequency response of the cavity. The bus model was created to be more similar to the measurement situation and also so that a comparison of the two different models could be done. The model was created by multiple boxes placed within a large box to be seen in Figure 3.1. Parts that were assumed to not have any acoustic effect in the desired frequency range, such as the handrail or details of the walls and the roof, were excluded. The dimensions of the model were based on measures from a CAD model of the same bus, and the utmost measures were also the same as for the model of the rectangular box.

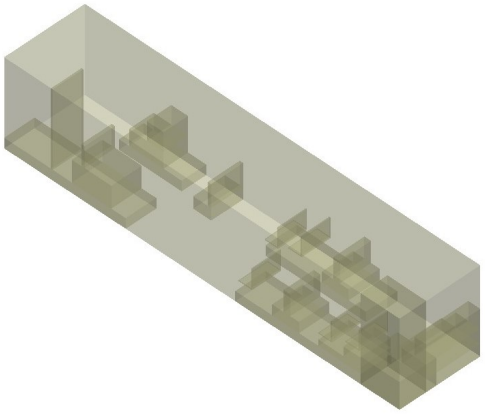

Figure 3.1: The boxes that the model is based on.

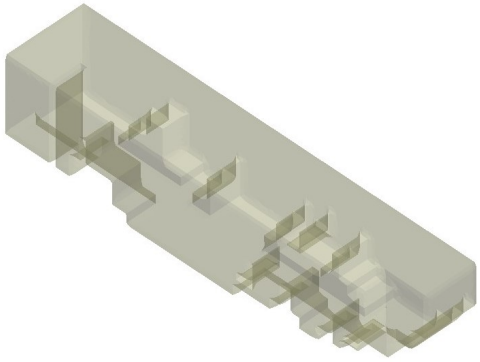

Figure 3.2: Volume mesh that represents the cavity of the bus.

The mesh of the model is fundamental to get results that can be trusted. Therefore, the elements of the mesh were studied for multiple combinations of settings for the three different meshes that result in the volume mesh, as seen in Figure 3.2 and more detailed in Figure 3.3. As presented in equation 2.7 at Section 2.3, an element size of 1.7 m is appropriate for frequencies up to 200 Hz with 8 elements per wavelength. To make sure that most of the elements were within the desired size, the settings were set to a finer value and the resulted mesh was studied so that the distribution of the mesh size was acceptable. Figure 3.4 shows that most of the elements are smaller than the required size; the mean edge length is about 0.12 m and the maximum is 0.2 m. The amount of elements that are too large is small enough to not have a significant effect on the results. The mesh consisted of 62650 nodes and 336863 elements, which is finer than the rectangular box model. The reason for the finer mesh is primary to get a mesh that follows the contours of the seats well, but also to get a representative estimation of the pressure distribution in the model. How this mesh was achieved, and with what settings, will now be explained step by step.

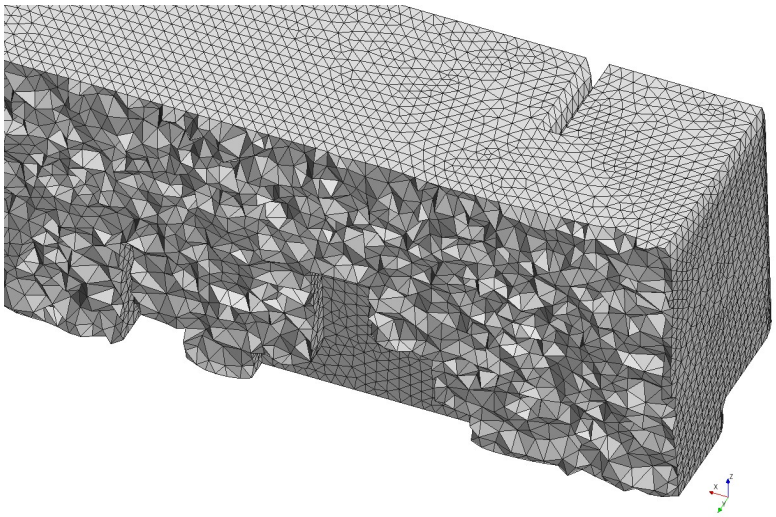

Figure 3.3: A cross section of the volume mesh in the front of the bus.

After the model was created by all the boxes a shrink wrap was made. This fills the cavity of the model following the outer shape of the boxes and the inner surface of the largest box, which represents the outer walls of the bus. The settings for this mesh were: element size 0.1 m, 0 m distance to the surrounding boxes and a minimum cavity of 3 m^3, to not fill the smaller boxes representing the seats. This mesh was then refined by a mesh on mesh, creating another 2D mesh with smoother corners and triangular elements; the element size was set to 0.1 m. At last, the created 2D mesh laid the basis for the created 3D volume mesh. The elements were triangular and the size was 0.14 m. The assigned properties of the medium inside were the ones for air: sound speed 340 $\frac{m}{s}$ and fluid density 1.225 $\frac{kg}{m^3}$.

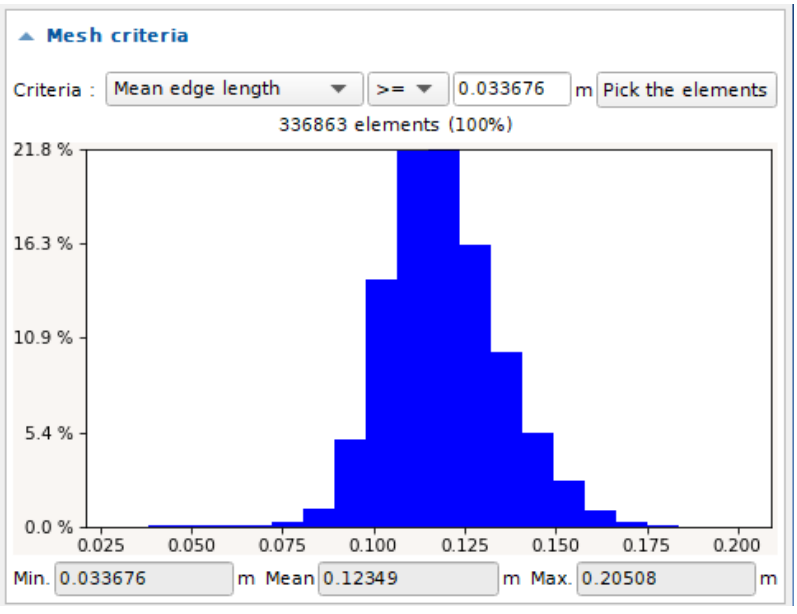

Figure 3.4: Size of the mesh elements in the volume mesh of the bus model.

When the final mesh was chosen, two different analyses were performed in *Actran*. For both analyses the boundaries were rigid, being the only influence of the cavity itself; structural effects and excitation from, e.g. the engine, were excluded from the analysis. The first analysis was a Modal Extraction, computing the uncoupled, closed cavity modes with no damping. This resulted in a list of the modes of the cavity, which were compared to the measurements but also with the rectangular box simulation.

Thereafter, a Direct Frequency Response analysis was performed. This analysis is a simulation of the FRF measurement so the microphones (blue points) and sources (green points) were placed in approximately the same positions as during the experiment, as can be seen in Figure 3.5 and Figure 3.6. The sources were defined as spherical volume acceleration sources with an amplitude of 1 $\frac{\mathrm{m}^3}{\mathrm{s}^2}$, and they were activated one by one. Multiple field points were defined in positions for all the different microphones. This results in the response at the microphones being calculated and later can be plotted in the *Actran* pre-processor, *PLTviewer*. The DFR was calculated for the frequency range of $1 - 200$ Hz with a frequency step of 0.25 Hz, just as the resolution for the experiment.

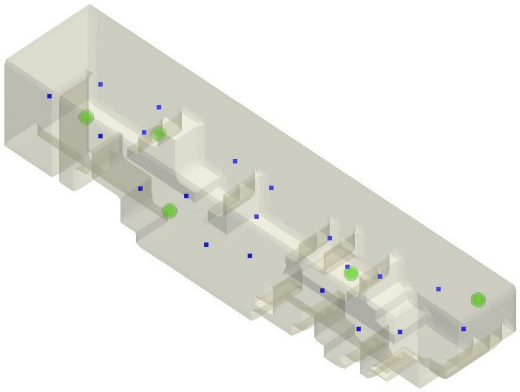

Figure 3.5: Positions of the microphones (blue) and sources (green) in the bus model.

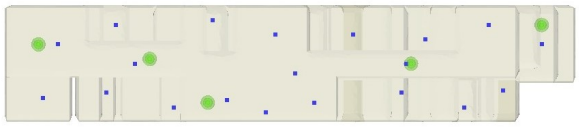

Figure 3.6: Microphone (blue) and source (green) positions in the bus model seen from above.

3.2 Sound Pressure Level Measurements

Interior Sound Pressure level measurements were performed according to a Volvo Bus Corporation (VBC) Test Code for interior noise and driveline vibrations, which is based on the Standard ISO-5281 [19]. The requirements stated in the Standard ISO-16121-4 [15] for the sound levels at the driving position were also used as reference but the measurement time was lower in this case. The measurements were performed in a complete bus in general good condition and production status at *Hällered Proving Ground*, a test track and proving ground owned by Volvo Car Group. A general view of the track can be seen in Figure 3.7, and Figure 3.8 shows the outside conditions during the test. The measurements were performed only on the two straights of the track which are highlighted, in Figure 3.7, as A and B to

avoid the influence of the engine load and the axles load; as during the turns, the outside wheels would turn quicker than the inner ones. The length of the straights limited the duration of the measurements, which was however never shorter than 30 seconds. The air temperature during the time of the measurement was between 4.1°C and 8.6°C and the average wind speed was 2 m/s. The temperature of the ground surface on site was between 1.9°C and 9.0°C and the road surface was clean and dry.

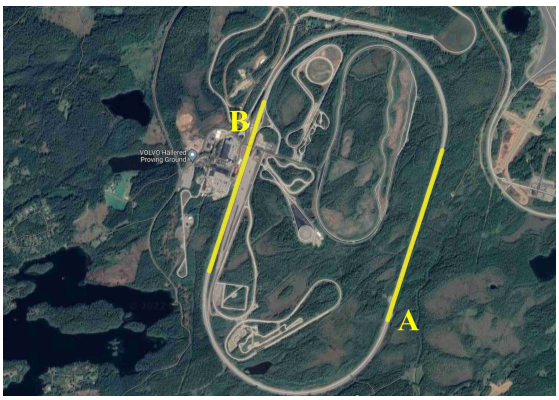

Figure 3.7: General view of Hällered Proving Ground, with the used tracks for the SPL measurements highlighted.
Picture from *Google Maps*.

Figure 3.8: General view of the exterior of the bus during the SPL measurements.

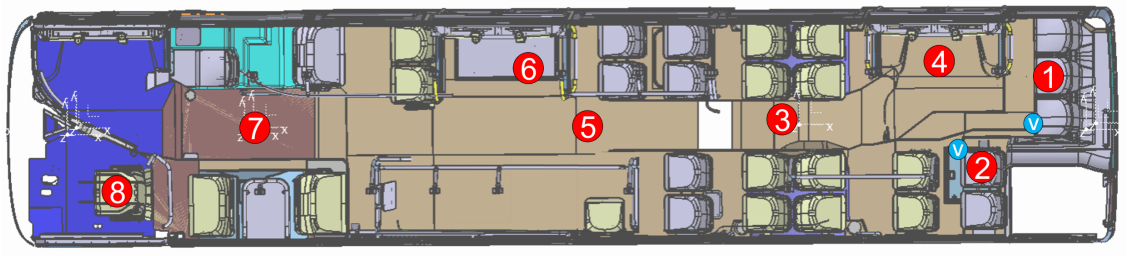

Figure 3.9: Top-view of the bus with an overview of microphone positions (red circles) and accelerometer positions (blue circles) for the SPL measurements.

The *Müller-BBM PAK* measurement system with the software *PAK 5.11* was used to record sound in the bus. The noise measurements were carried out with a sampling frequency of 44.1 kHz. Eight free-field microphones distributed along the bus, placed in representative positions as shown in Figure 3.9, were used to measure the SPL in the cabin. The height of the microphones for the standing passenger positions ranged between 1.4 m and 1.8 m and that for the seated passenger positions was approximately 0.7 m above the seat cushion, measured as observed in the diagram in Figure 3.10. Pictures of the setup of each of them, the description of the microphone positions and their exact heights are shown and described in Appendix B. In addition, the vibrations were also measured at two points at the back of the bus to identify the main vibrations of the structure. Two triaxial accelerometers were

used and their placement can be seen in Figure B.21 and Figure B.22 of the same appendix. The vibration measurements were performed with the same measurement system and also a sampling frequency of 44.1 kHz.

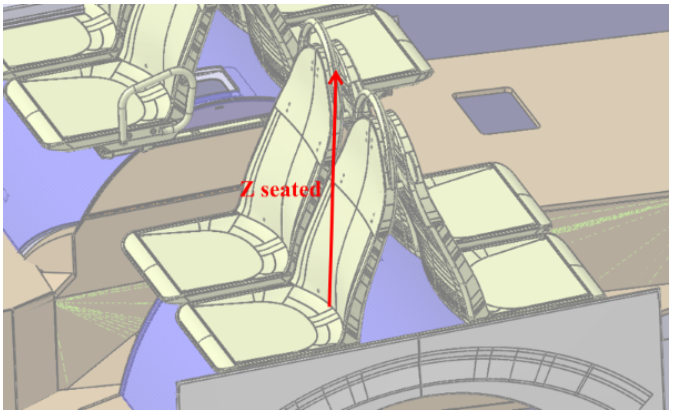

Figure 3.10: Microphone height for seated passenger positions.

Several test cases were performed on the bus to gain a better understanding of the sound levels and noise sources. They are listed and described below.

- Wide Open Throttle acceleration (WOT): The throttle is fully depressed from standstill condition to maximum speed.
- Rollout in neutral gear and gear D: The throttle is fully released starting at maximum speed (80 km/h) until the vehicle is at standstill.
- Constant speeds: 20 km/h, 30 km/h, 40 km/h, 50 km/h, 60 km/h, 70 km/h and 80 km/h.
- Low idle. With and without air compressor charging.
- Low idle sweep: Full engine RPM sweep is performed from low idle to maximum engine speed and consecutively from maximum to minimum engine speed and then low idle. With and without air compressor charging.

3.2.1 Post-Processing

After all the measurements were finished, a post-processing of the data was performed also in *PAK*. All test cases and microphone positions, as well as the vibration results, were investigated to get a first impression of the frequencies with higher levels, and a better understanding of the most relevant noise sources in the cabin.

Firstly, the Equivalent Continuous A-weighted Sound Pressure Level over time, $L_{Aeq,T}$, was calculated for all constant speeds and the two low idle cases (with and without compressor), as it is a good indicator of the actual exposure of passengers and drivers to noise. To calculate these levels at the constant speed cases, first, the two measurements performed for each test case were averaged and then the A-weighted SPL were averaged over time to obtain a single value per speed and microphone position.

Secondly, FFT was performed for all test cases to find the first resonances in the cabin, for both noise and vibration measurements. A zero-padding factor of 4 and a block size of 1024 were used to calculate the FFT and the data was resampled with a sampling frequency of 1000 Hz to gain a higher frequency resolution at low frequencies, as they are the ones of interest. A Hanning window was applied to avoid spectral leakage.

Lastly, an order analysis related to the engine speed was made for the rollout and WOT test cases to search for the strongest engine orders and their frequencies, as well as variations in SPL and noise sources depending on the speed and the microphone positions. For this purpose, the same settings as for the FFT were used: sampling frequency of 1000 Hz and blocksize of 1024 points. In addition, maximum order of 10 was selected for the final analysis presented in this thesis due to the frequency range of interest, but higher orders were observed as well to get a sense of other noise sources at higher frequencies.

3.3 Frequency Response Function Measurements

Acoustic FRF measurements were performed inside the bus to find the main first resonances in the cabin. For this purpose, a low frequency monopole source (Q-source) was used as the excitation source, as described in Section 2.5. The sound field produced by the source, in this case, was white noise with a level of 5 V and frequency content between 10 Hz and 1000 Hz. In addition, amplification of 20 dB was used to achieve higher sound pressure levels. Regarding the measurement parameters, different block lengths and number of averages were tried to obtain the best compromise between clear resonance peaks, good coherence and measurement time, and the ones shown in Table 3.1 were finally selected. This table includes also a summary of the source settings mentioned above. Moreover, five different source positions were selected to excite as many modes as possible. To achieve this, they were also positioned at different heights, which are described in Table B.2 of Appendix B.

Table 3.1: Input source parameters and FRF measurement settings.

Source parameters		Measurement parameters	
Type of noise	white noise	Bandwidth (Hz)	512
Level (V)	5	Sampling Freq. (Hz)	1024
Freq. definition (Hz)	10 - 1000	Window	Hanning
Signal duration (s)	120 (4 s x 30 avg.)	Blocklength (points)	2048
Amplification gain (dB)	20	Freq. Resolution (Hz)	0.25
		Number of averages	30
		FRF estimator	H1

Regarding the outputs, 20 free-field microphones of the same type were distributed along the bus, considering all the different areas and types of seats on the bus. An

overview of both the sources and microphones can be seen in Figure 3.11, where the red points correspond to the microphone positions also used in the SPL measurement and the orange ones are those used only for the FRF measurement. The heights of the microphones were chosen to take into account common heights of people and they ranged between 0.5 m and 0.9 m above the seat for the seated positions and between approximately 1.5 m and 1.8 m for standing positions. A general view of the interior of the bus with all the microphones positioned can be seen in Figure 3.12 and the description of these positions and their exact heights, as well as pictures of each setup, are described in Appendix B.

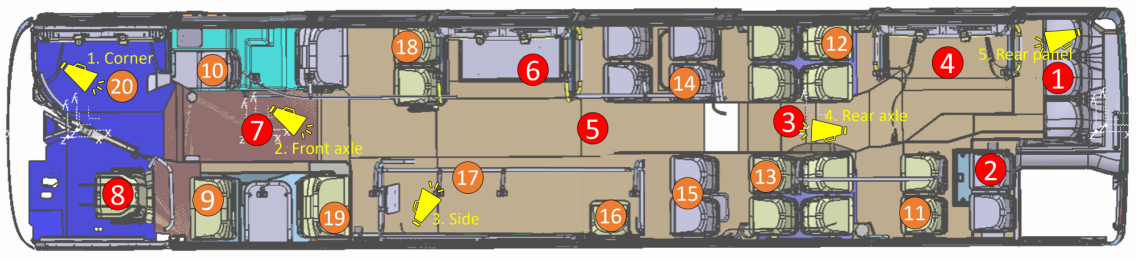

Figure 3.11: Overview of source and microphone positions for the FRF measurements. The red circles are the same microphone positions as in SPL and the orange ones are only used for FRF measurements. The sources are seen in yellow.

Due to meteorological conditions, the test was carried out indoors, close to a workshop but in a separate room that can be seen in Figure 3.13. No remarkable noises were present, the ventilation was turned off and all possible doors closed. However, noise from a pipe could be heard and some inaudible low frequency noise was also visible in the results. Figure 3.14 shows an example of SNR for one of the measurement settings (source 1, microphone 5). It can be observed that while at higher frequencies the SNR is quite high, it is slightly decreased at low frequencies, approximately below 50 Hz. In addition, at 50 Hz and 100 Hz, there are peaks in the background spectra, which correspond to the power supply.

Figure 3.12: General view of the interior of the bus during FRF measurements.

Figure 3.13: General view of the exterior of the bus during FRF measurements.

Additionally, four different measurements were performed for each source position with the same setup to ensure that the conditions at the measurement site were the same and to avoid isolated noises that could negatively affect the results. In Figure 3.15 the acoustic FRF of source 1 and microphone 1 is presented as an example to demonstrate that the results were nearly identical for the four runs in the analysed frequency range. This was fulfilled for all other measurement configurations as well.

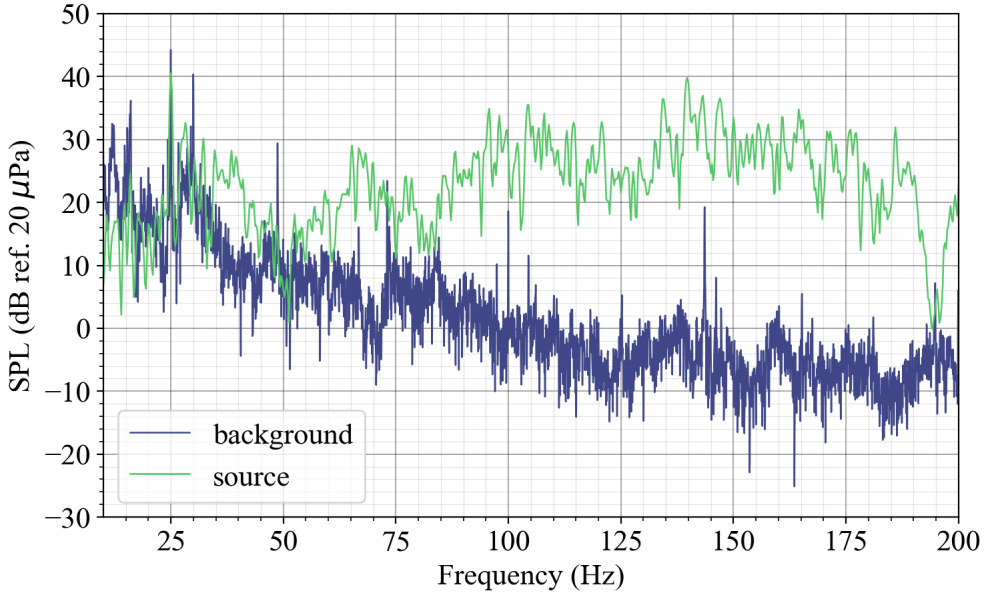

Figure 3.14: Spectra of a noise measurement (source 1, microphone 5) and a background noise measurement.

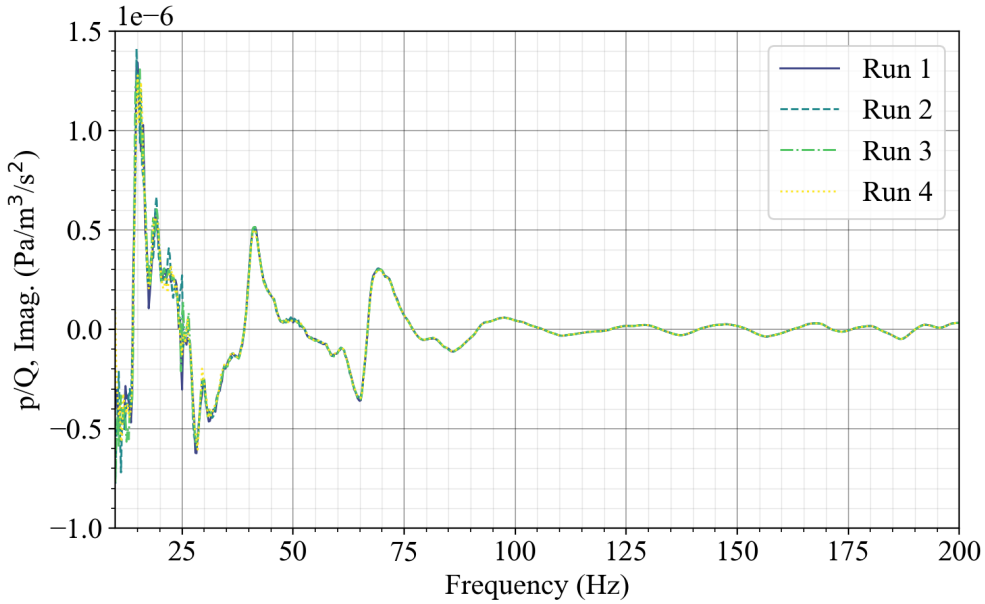

Figure 3.15: Acoustic FRF response of four measurements performed with the same configuration for source 1 and microphone 1.

4

Results and Discussion

The objective of this thesis is to compare the resonances found in both simulations and measurements in the cavity of a bus cabin; as well as to gain a better understanding of the different types of modes in the bus and noise sources that could amplify the levels at those frequencies. For this purpose, the results of simulations, SPL measurements and FRF measurements are presented and discussed in this chapter, followed by a comparison of the resonances obtained with the different methods.

4.1 Simulation

The results from the simulations are presented and discussed in three parts: modal response of a rectangular box with the same dimensions as the bus, modal response of the bus model, and simulated frequency response of the bus model.

4.1.1 Modal Response of a Rectangular Box

There are in total 100 modes below 200 Hz, according to Equation 2.3, but only the first ones are described in this section. The first 10 modes with their frequencies and type of mode are listed in Table 4.1. The table shows that the first four modes are axial along the length of the bus, referred to as x-direction in Figure 2.2. The fifth mode is tangential in the z-direction, which corresponds to the height of the bus, and mode seven is in the y-direction, the width of the bus. The sixth mode and those above seven are mostly tangential and oblique. The visualization of the ten first modes can be found in Appendix C, where they are compared with the bus model results, which are further discussed in Section 4.1.2.

Table 4.1: First analytical modes of a box with the same dimensions than the bus under test.

Number	Freq. (Hz)	Mode	Type	Number	Freq. (Hz)	Mode	Type
1	14.41	1-0-0	ax	6	67.73	1-0-1	tan
2	28.82	2-0-0	ax	7	70.58	0-1-0	ax
3	43.23	3-0-0	ax	8	72.04	1-1-0	tan
4	57.65	4-0-0	ax	9	72.08	5-0-0	ax
5	66.18	0-0-1	ax	10	72.20	2-0-1	tan

4.1.2 Modal Response of the Bus Model

The modal extraction of the bus model resulted in 94 modes below 200 Hz. The first 20 of them are found, together with the frequencies of the modes for the rectangular box model, in Table 4.2. The inner dimensions of this model are different from the rectangular box model, due to the added seats, which affect the eigenfrequencies and mode shapes. What is interesting from the table is that the frequencies are not significantly different; they differ about 3 Hz at most for the 20 first modes and no difference between the higher and lower frequencies occurred. These results are consistent with those from [20], where the modal response with or without seats in a minivan was compared, which is also the main difference between these two models.

Table 4.2: First analytical modes of the bus model and the rectangular box.

Mode number	Bus model Freq. (Hz)	Rectangular box Freq. (Hz)	Mode number	Bus model Freq. (Hz)	Rectangular box Freq. (Hz)
1	14.47	14.41	11	76.25	76.25
2	26.50	28.82	12	79.49	79.08
3	41.30	43.23	13	82.47	82.80
4	54.10	57.65	14	87.16	86.52
5	63.91	66.18	15	89.99	87.81
6	68.85	67.73	16	91.24	91.18
7	70.78	70.58	17	94.85	96.81
8	71.83	72.04	18	98.01	97.88
9	72.18	72.08	19	99.88	97.92
10	74.38	72.20	20	102.23	100.95

Figure 4.1 and Figure 4.2 show that the second mode is axial for both models. This suggests that the removed volumes in the bus model compared to the rectangular box one do not significantly affect the modes in the length direction, which are the most efficient modes to excite in accordance with [3]. There is only a slight change of frequency but the shape is basically the same. The first four modes are practically the same in this model as in the rectangular box model, as seen in the ten first modes visualized in Appendix C. This was expected because the modes at higher frequencies will be affected by the smaller shapes due to their shorter wavelength.

Figure 4.3 and Figure 4.4 show the fifth mode for the rectangular box and bus model respectively, which is the first mode that differs between the two different models. This is because the standing wave that occurs in the z-direction is highly affected by the added seats and floors in the bus model. Hence, the pressure distribution is not symmetrical and the type of mode is not obvious for the bus model. Likewise, this applies to the sixth mode in Figure C.12 found in Appendix C, where the pressure distribution does not indicate any pattern throughout the bus.

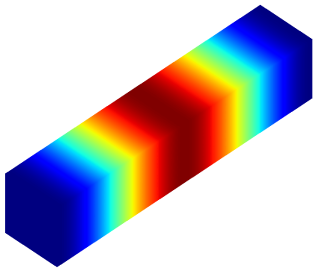

Figure 4.1: Box mode 2, f = 28.82 Hz.

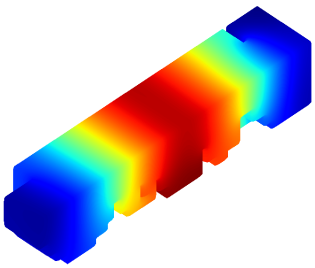

Figure 4.2: Bus mode 2, f = 26.50 Hz.

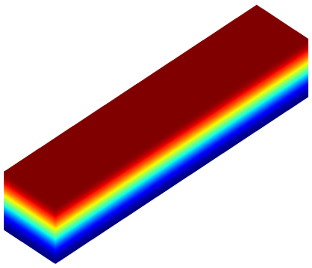

Figure 4.3: Box mode 5, f = 66.18 Hz.

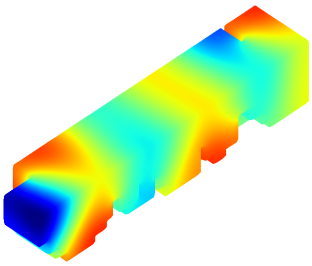

Figure 4.4: Bus mode 5, f = 63.91 Hz.

Even though the mode shapes do not indicate as clear peaks as the analytical solution for many of the modes (e.g. 6, 7, 8), some modes have considerable similarities with the rectangular box modes, even at higher frequencies. Namely mode 9, shown in Figure 4.5 and Figure 4.6, but also mode 10 as seen in Appendix C. Hence, the results from this analysis confirm that the source positions displayed in Figure 3.11 should be theoretically sufficient to excite the modes of the bus cavity.

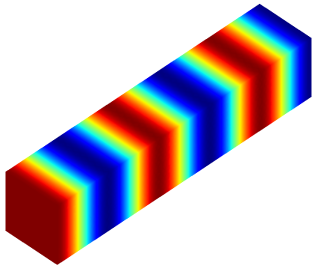

Figure 4.5: Box mode 9, f = 72.08 Hz.

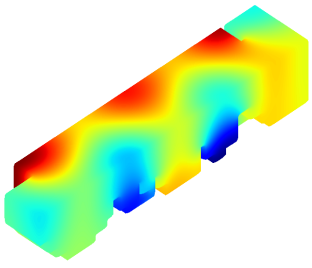

Figure 4.6: Bus mode 9, f = 72.18 Hz.

The difference in the eigenfrequencies is relatively small for the first 10 modes, but the mode shapes differ to a greater extent. It could be possible that the rectangular box model gives enough information in many cases, one being the assessment of where to place sources to excite the cavity. However, the results from the bus model will be the ones further discussed and compared to the measurement results since they will theoretically be closer to them.

4.1.3 Frequency Response of the Bus Model

The results from the direct frequency response are shown in Figure 4.7 for source 1, placed in the front corner. It is visible that the peaks get closer with the increased frequency making it difficult to separate and identify them, just as expected from the results shown in Table 4.2. Therefore, the peaks up until 100 Hz will from now on be analysed in further detail and compared with the measurement results.

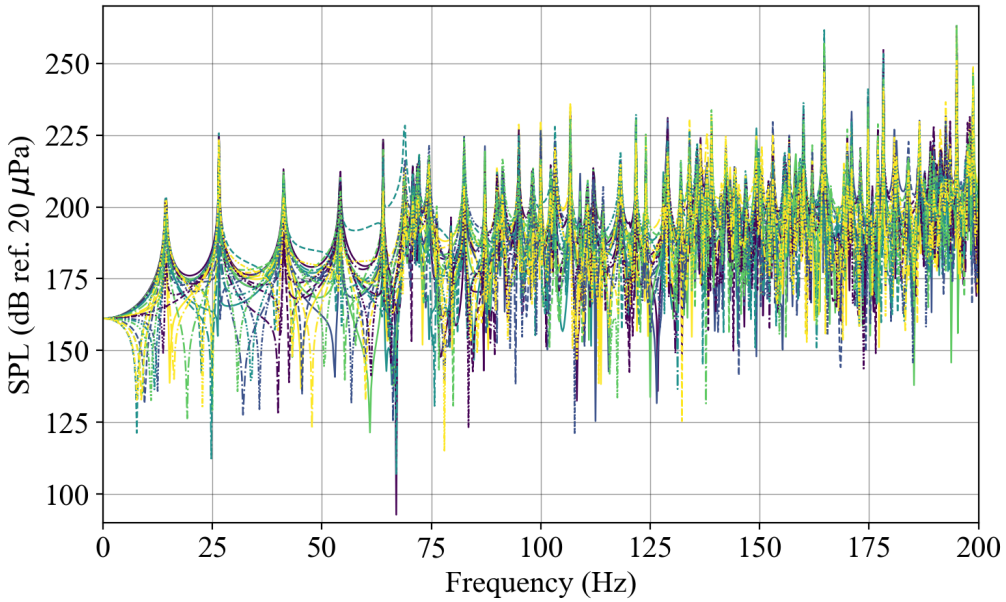

Figure 4.7: Frequency response in the bus model with source 1 at the corner activated up until 200 Hz.

The aim is to determine where the resonances occur; that is the reason for all the sources and microphones being presented in the same graph, see Figure 4.8. The results for one source position at the time are presented in Appendix D, where it is clear that all the resonant peaks are visible for all the source positions; but the amplitude differs for some of them. In contrast with the expected theoretical results, source positions two and three resulted in really good peaks in the simulations when one and five were expected to be the best due to their corner positions. This difference is not significant enough for other source positions to be suggested, but this will be further discussed in Section 4.3. However, it is natural that all the modes are not equally excited for all of the source positions due to the pressure distribution.

In Figure 4.8 it is possible to conclude that the source positions are theoretically efficient to excite all the resonant frequencies below 100 Hz. This can be said because the peaks coincide with the red vertical lines that are the frequencies from the modal extraction. After all, this is a simulation with rigid boundaries which only results in how the cavity is affected by the excitation and the correlation was expected.

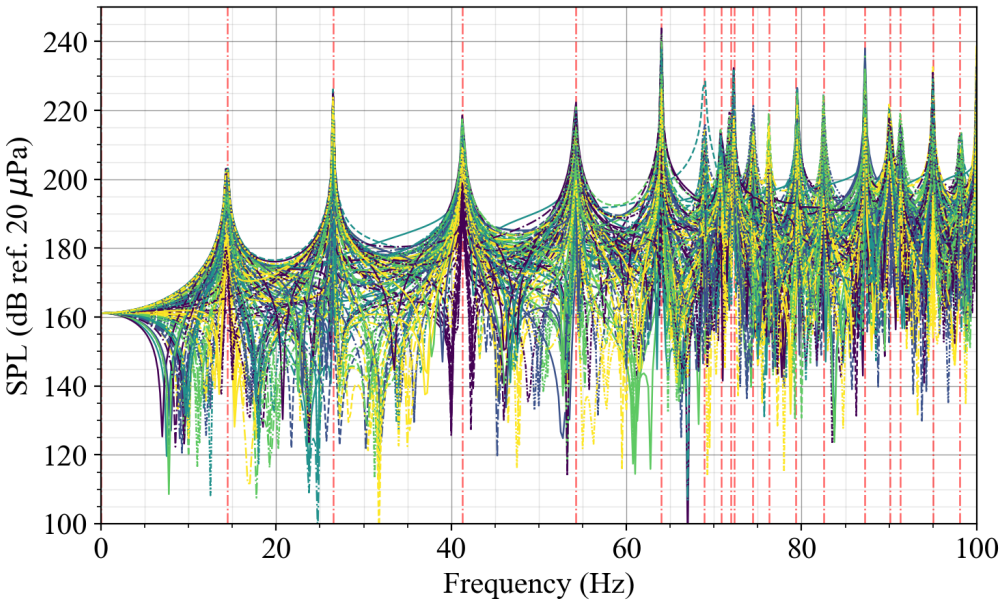

Figure 4.8: Frequency response in the bus model for all sources and microphones. The dash-dotted vertical red lines correspond to the frequencies of the modes from the modal extraction.

4.2 Sound Pressure Level Measurements

In this section, the results of the different analyses performed on the signals of the SPL measurements in operation are shown and discussed. Firstly, the Equivalent Continuous Sound Pressure Levels of the constant vehicle speeds and low idle cases; secondly, an FFT analysis; and lastly, an order analysis based on the engine speed.

4.2.1 Equivalent Sound Pressure Levels

The equivalent continuous A-weighted Sound Pressure Level, over the complete duration of each measurement T, $L_{Aeq,T}$, was calculated for all constant speeds and low idle cases for all microphone positions; the results are shown in Table 4.3. For the constant speeds, it can be easily observed that the levels increase with velocity for all microphone positions. The positions that present higher levels are the *Rear Bench* (1) and the *Driveline* (2), as highlighted in the table. The *Rear Axle* (3) and *Rear Door* (4) microphones show also higher levels than the rest of the positions in the middle and front of the bus. In the low idle cases, the *Rear Bench* is also the location with the highest levels, followed by the *Rear Door*. This indicates that the main noise sources are located at the back of the bus cabin, which correlates also with the subjective impression. It has to be taken into account that one hatch at the left of the rear bench was missing during the measurements, as can be seen in Figure B.1, which led to an increase in sound levels at those positions due to insufficient insulation.

On the contrary, the location in the bus where the SPL is lowest is the *Drivers ear* (8), which presents a reduction of between 3 dB and 8 dB depending on the test

case compared to the highest levels. The sound level requirements stated in [15] to achieve good comfort conditions for the driver are $L_{Aeq,T} \leq 70$ dBA for 50 km/h, and $L_{Aeq,T} \leq 60$ dBA for low idle. These are fulfilled, as the levels at these cases are 66.8 dBA and 54.2 dBA to 55.0 dBA respectively. This indicates that the exposure of the driver to workplace noise is reasonable.

Table 4.3: Equivalent Continuous A-weighted SPL over time, $L_{Aeq,T}$, for all constant speeds and microphone positions. The microphone position with highest SPL is highlighted for every test case.

$L_{Aeq,T}$, dB(A)									
Measurement position	Constant speed (km/h)							Low idle	
	20	30	40	50	60	70	80	compr.	no compr.
1. Rear bench	67.8	69.2	69.5	71.1	72.6	75.5	78.5	67.0	66.6
2. Driveline	66.3	67.6	68.2	70.3	71.9	75.7	78.1	65.2	64.9
3. Rear axle	64.1	66.1	67.4	70.3	71.7	74.5	77.8	64.4	63.5
4. Rear door	66.5	68.2	68.8	70.7	71.9	75.5	77.4	66.1	65.5
5. Between axles	62.5	64.7	66.8	70.2	70.8	74.1	76.9	61.1	60.8
6. Mid door	61.6	63.5	66.0	68.2	70.0	73.4	77.3	59.7	59.1
7. Front axle	60.8	62.7	65.3	68.0	70.2	72.0	76.1	58.2	57.3
8. Drivers ear	60.0	61.3	64.0	66.8	69.4	71.9	73.8	55.0	54.2

4.2.2 FFT Analysis

There are multiple noise sources which may contribute to the interior noise in a bus; some of them are produced inside the cabin due to its properties, dimensions or materials, but most of them are originated outside and generated by the interaction with the structure of the bus, causing either airborne noise or structure-borne noise when transmitted to the cavity. At the same time, these may excite the cavity modes at some frequencies and therefore amplify their amplitudes.

An important vehicle noise source is the one produced by the contact between road and tyre: road noise. The vibration of the tyre is transmitted to the interior of the cabin through different paths as the suspension or panels. In this case, the structure-borne noise is the dominant one below approximately 400 Hz [21], so it has to be taken into account for the analysis of the results presented in this section. Structure-borne noise can also be produced by other sources such as the engine, causing for instance engine boom noise below 100 Hz. In addition, the tyre rotation can also cause structure-borne noises, especially if unbalances are produced. Taking into account the tyre size of the bus under test, the theoretical tyre rotation frequency ranges between approximately 2 Hz and 7 Hz depending on the vehicle speed, as calculated in Appendix F. Another common noise source in a vehicle is wind noise, which is relevant mainly at high frequencies and high vehicle speeds. Moreover,

power train noise or brake noise may also affect the noise levels, but they are not analyzed in this report as not sufficient tests were performed to be able to separate all noise sources.

Taking into account the potential noise sources and frequencies described above, FFT was performed to convert all signals to the frequency domain in order to observe the resonant peaks in the bus cabin and to understand which types of modes are present and which noise sources may be amplifying them. This analysis was conducted for all test cases and the resulting plots between 0 Hz and 100 Hz are shown first for three different constant speeds, secondly for the low idle cases and lastly for the rollout measurements. The rest of the test cases show similarities with the ones presented in this section, and will therefore not be discussed further here; they can be observed in Appendix E. Also, a table with the encountered peaks for every test case is presented in Appendix I.

First of all, with the selected FFT settings, all peaks are clearly visible in the frequency range of interest; being approximately at the same frequencies for all microphone positions. The analysis will be therefore focused on these frequencies and not on the individual differences between positions in the bus. In Figure 4.9, the results are presented for 20 km/h, 50 km/h and 80 km/h. When observing the three plots, it is clear that the overall sound level increases when increasing the vehicle speed, especially at frequencies above 40 Hz. This can be due to the structure-borne road noise, which is higher for higher speeds. In addition, as the doors of a bus are not as sealed as, for example, the ones in a car, the road noise can also be transmitted as airborne noise inside the cabin, increasing also the overall level.

Most of the peaks coincide for the different vehicle speeds. However, the ones with the highest amplitude vary between test cases. When driving at 20 km/h the peaks with the highest amplitudes are at 37.6 Hz and 75.4 Hz, which correspond to the second and fourth orders of the engine (1100 RPM). At 50 km/h, the largest one is at 45.2 Hz; and at 80 km/h, the more evident resonance frequency is the one at 71.3 Hz. These two also correspond with the second order as the engine speed for 50 km/h and 80 km/h is 1338 RPM and 2136 RPM respectively. Additionally, in the results obtained from the accelerometers, peaks at the same frequencies were also present, which indicates that vibrations are transmitted as structure-borne noise through the structure to the bus cavity. More information about the orders of the engine can be found in Section 4.2.3, where an order analysis is shown.

Moreover, at really low frequencies, there is a small peak of approximately 65 dB to 70 dB. At a constant speed of 20 km/h, this resonance occurs at 2 Hz, and then it moves towards higher frequencies for higher constant speeds; for instance, at 50 km/h it is at 4.6 Hz. At higher constant speeds of 70 km/h to 80 km/h this peak is even higher and coincides with the next one at approximately 7.5 Hz so it can not be longer clearly observed. These frequencies for the different speeds correspond with the theoretical values of the tyre rotation frequency, which indicates that this noise source is also influencing the noise levels in the cabin.

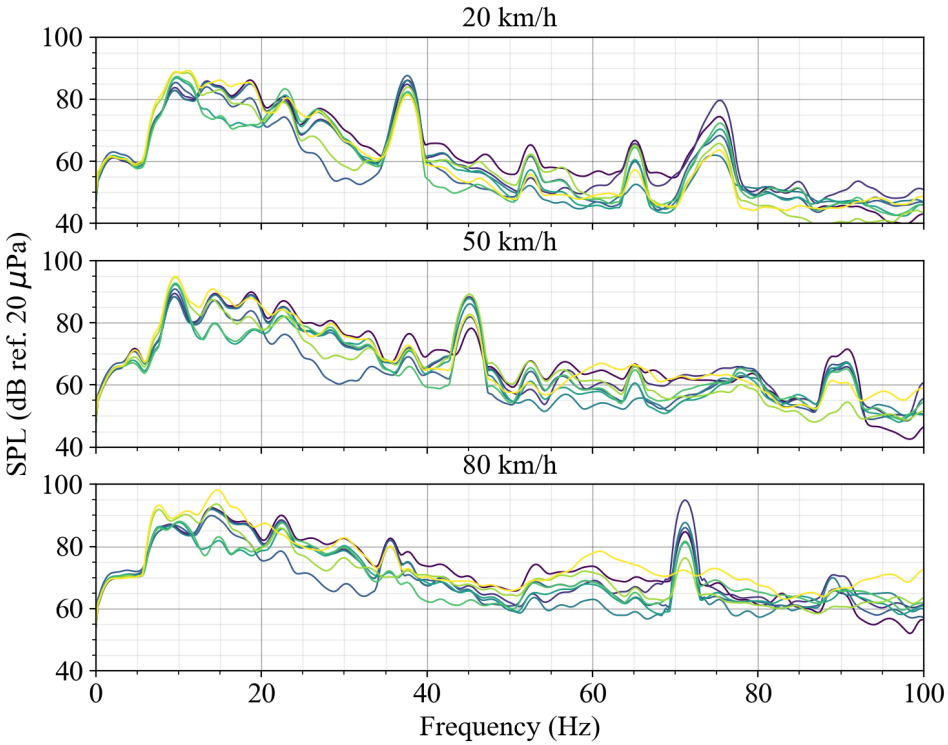

Figure 4.9: FFT for 20 km/h, 50 km/h and 80 km/h and all microphone positions.

In Figure 4.10, the sound pressure levels for the low idle cases, both with the compressor running and without it are shown. Clear peaks can be observed, and they are approximately at the same frequencies as the ones at constant speeds or WOT, but the road/tyre noise is non-existent, and consequently neither is the structure-borne noise transmitted from the contact between road and tyres. This makes the overall noise levels lower, thus enhancing the resonances due to the cavity and the structure. For both cases, there is a large peak at 11.7 Hz, which corresponds exactly to the engine rotation frequency, that is 700 RPM when idling; and another peak at 23.2 Hz, which relates to its first harmonic.

Comparing the results with and without the compressor, it can be seen that although the peak occurring at 41.7 Hz is present at both conditions, the sound pressure level at this frequency is significantly reduced when the compressor is off. This effect occurs also in the low idle sweep test case, shown in Figure E.6 at Appendix E, which indicates that the noise produced by the compressor amplifies the mode at this frequency.

Lastly, the rollout SPL are shown in Figure 4.11. At the rollout plots in *Neutral* (N), a peak can be observed at 23.4 Hz. As it occurs in the low idle cases, the engine speed is 700 RPM here, corresponding also this peak with the second order of the engine. At higher frequencies, the overall level decreases and there are no more relevant peaks. During rollout in *Drive* mode (D), however, the engine speed is not constant, but decreases with time and varies with the engine breaking as well, as can be observed later in Figure 4.13. As said before, the engine rotation while driving ranges between 1100 RPM at 20 km/h and 2136 RPM at 80 km/h, which

corresponds to the frequency range 18 Hz to 36 Hz. This results in the noise being distributed over this frequency range and in less clear resonances, contrary to the above cases.

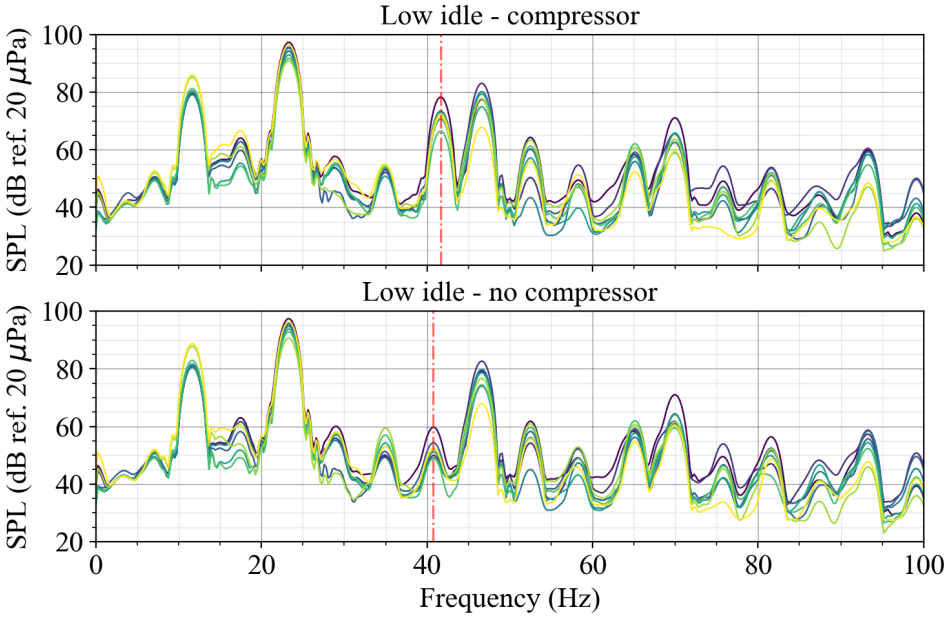

Figure 4.10: FFT for the low idle test case with compressor and without compressor for all microphone positions. The dash-dotted vertical red lines correspond to the resonance which presents the most evident variation between both test cases.

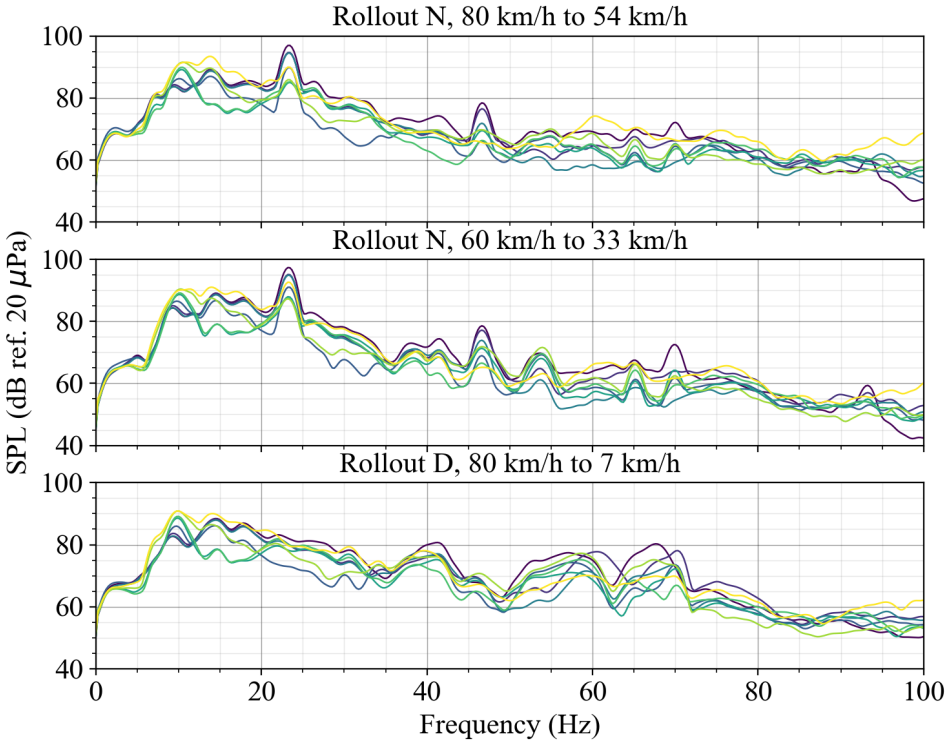

Figure 4.11: FFT for the rollout for all microphone positions.

4.2.3 FFT over Vehicle Speed and Order Analysis

In this section, the FFT over vehicle speed and the order analysis for the WOT case is presented to get a further understanding of which frequency range of the engine affects the noise level in the cabin. The results are shown from microphone position *Rear Bench*, hence it has the highest sound pressure levels according to Table 4.3. The same diagrams for the rollout cases can be found in Appendix G.

In the left graph of Figure 4.12, which corresponds to the FFT over vehicle speed, the frequency sweeps due to the increased speed are visible. Noise that does not have a clear relation between speed, frequency and order will not be discussed here since it is mentioned in Section 4.2.2. The main noise content in the spectrum is clearly visible as diagonal lines that are increasing with frequency due to the ramp-up of the engine and split into three major parts due to the gear change. This speed-dependent noise content is the frequency range from 40 Hz to 70 Hz so it is of importance since it has the potential to excite the modes in the cavity in the frequency range of interest. Which mode will be affected is dependent on the speed of the engine and its coupling to the body of the vehicle.

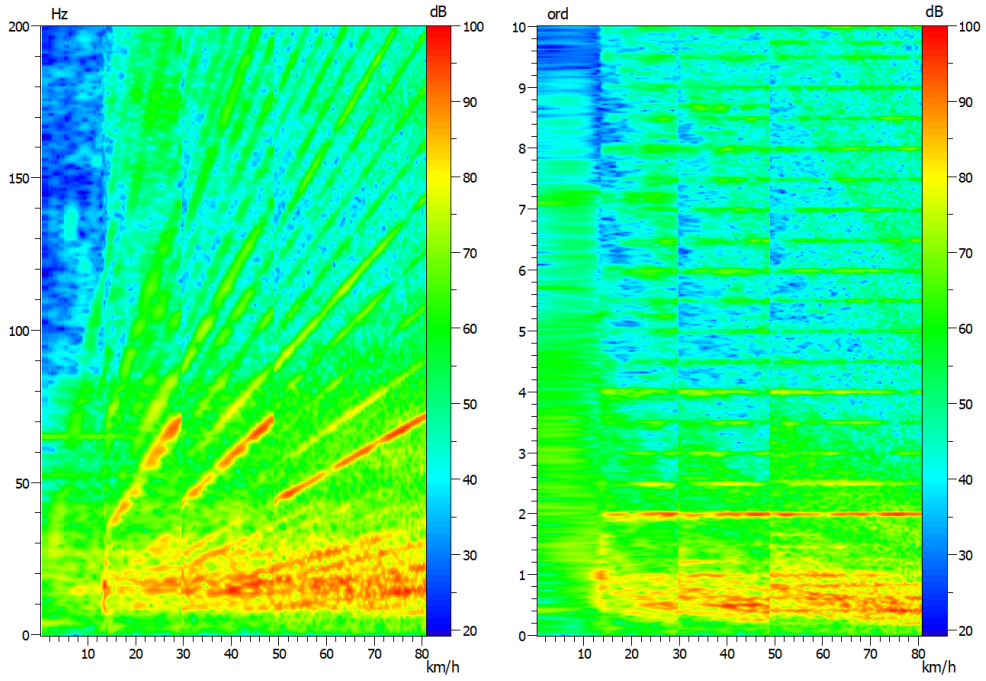

Figure 4.12: FFT over vehicle speed (left) and Order analysis (right) for WOT at rear bench.

As seen in Figure 4.13 the WOT driving case includes almost the complete range of operational speeds for the engine; only the low idle sweep has higher RPM. That is the reason for only showing this graph in this section. The lowest speed of the engine occurs when the vehicle is still before the full open throttle, the WOT case, at 550 RPM. The highest RPM is found in the peak of the low idle sweep at

2360 RPM, due to the full open throttle and no load on the output shaft. These RPMs correspond to a frequency range between 9 Hz and 50 Hz, where a considerable amount of noise is visible in both of the spectra in Figure 4.12. However, this is not related to the order of the engine and will not be discussed further in this section.

In the right graph of Figure 4.12 the order analysis is presented. The second order of the engine is visible, as well as the shift of gear around 10 km/h, 30 km/h and 50 km/h. The second order is dominant independently of the gear due to the four-cylinder diesel engine, which fires two cylinders at two times for each rotation of the engine. The frequency range of this order is approximately from 25 Hz to 70 Hz due to the acceleration. The fourth order is also significant for this type of engine, and it is more clear in the rollout cases presented in Appendix G. Since further measurements isolating separate parts have not been done it is not possible to relate the noise visible in these diagrams to other rotating sources than the engine. A recommendation for future work would be to include more parameters from the vehicle data, as well as a larger amount of accelerometers, to connect noise to their separate sources, but that has not been the main scope of this thesis.

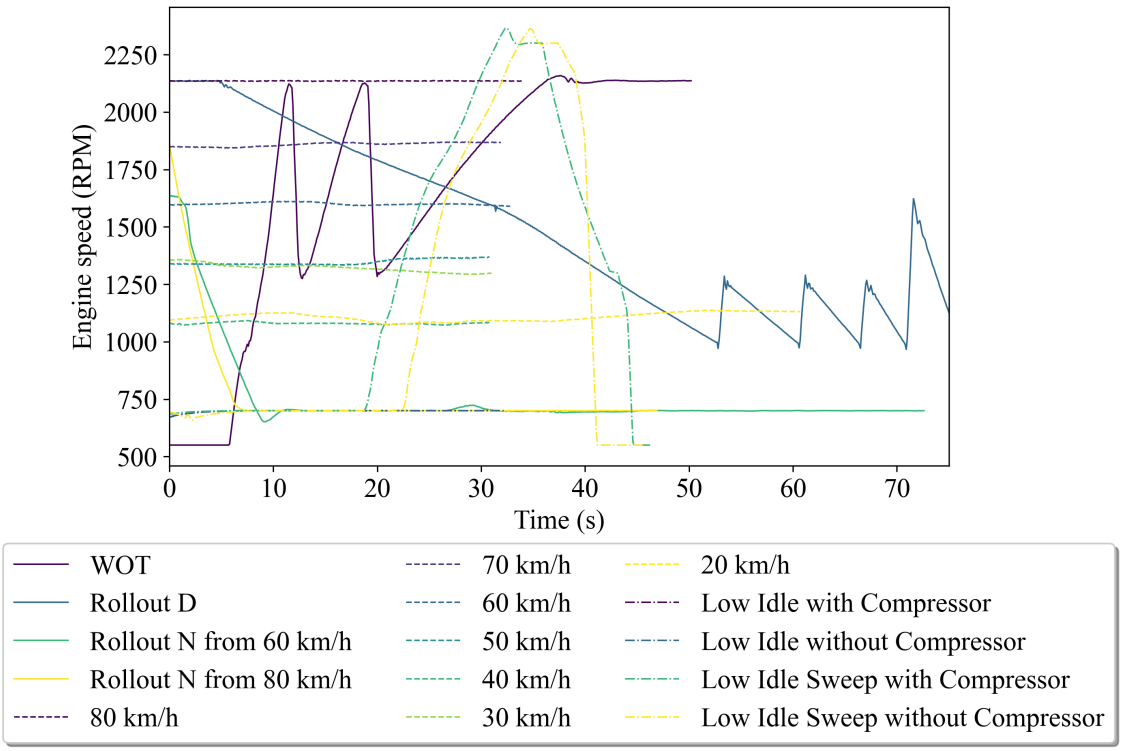

Figure 4.13: RPM of the engine during the different driving cases.

4.3 Frequency Response Function Measurements

Because of the described in Section 2.5, the FRF results are shown and discussed in this section and the resonance peaks are obtained based on the imaginary plots. Figure H.1 at Appendix H shows the FRF results for all sources between 0 Hz and 200 Hz. However, it can be seen that there is a high background noise below

10 Hz, which is due to the frequency response of the loudspeaker, as well as to the lower limit of the operational frequency range of the microphones, which is 20 Hz. Moreover, the levels are in general really low above 100 Hz and the peaks vary more between measurement configurations, which makes it more complicated to detect possible resonant frequencies, as occurred also in the simulation results described in Section 4.1.2. Because of this, the results are shown between 10 Hz and 100 Hz in this section. One coherence plot is shown in Figure 4.14 for source 1 and some microphone positions for the complete bandwidth of the measurements. It can be observed that except for some dips corresponding to the resonances in the bus, the coherence presents values close to 1 between 10 Hz and approximately 450 Hz, which indicates general reliability of the results in the frequency range of interest.

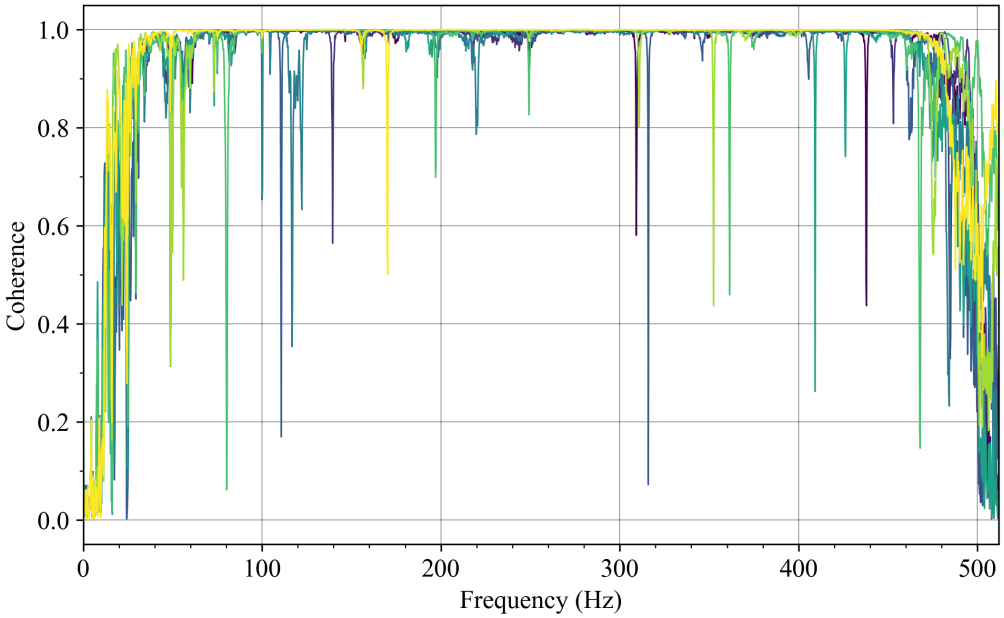

Figure 4.14: Coherence of some microphone positions and source 1.

The focus of this analysis is not the individual response of each configuration but the overall shape of all curves together. In Figure 4.15, the Frequency Response Functions are presented for all microphone and source positions. The vertical red lines correspond to the main peaks (and dips) that can be detected in this figure, which are also listed in Table 4.4. The resonant frequencies with the highest amplitudes occur at 14.7 Hz and 16.2 Hz, corresponding the first one to the first axial cavity mode in the length direction observed in the simulation (Section 4.1.2). The second one does not correlate with any mode found in the simulation, but it does with the SPL measurements, which indicates that it is a mode transmitted by the structure of the bus. However, before these frequencies, it is possible to distinguish also a smaller resonance around 11.5 Hz, which could be due to the excitation of the structure, as it occurs below the first simulated cavity noise. There are also some other resonances with high amplitudes at 19.3 Hz, 28.7 Hz, 31.0 Hz and 68.2 Hz, while the rest are smaller or with higher damping. The reasons for some of these small peaks may be the effect of the absorbing material present in the bus, both the

fabric covering the seats and the sound absorbers installed in the engine compartment, as well as an insufficient excitation of the source. The possible noise sources and the correlation with the modes obtained in the simulation are described further in Section 4.4, where the results of simulations and measurements are compared.

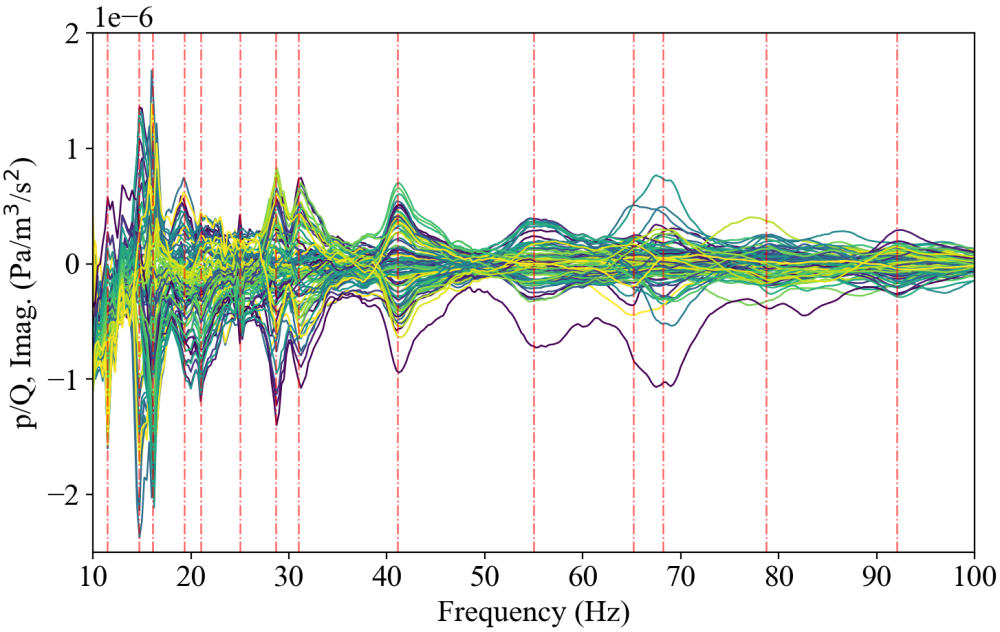

Figure 4.15: Imaginary part of the FRF measurement results for all sources. The dash-dotted vertical red lines correspond to the higher resonant frequencies.

Table 4.4: Resonant frequencies detected in the FRF curves in the range 10 Hz-100 Hz for all sources.

Peak	1	2	3	4	5	6	7	8	9	10	11	12	13	14
Freq. (Hz)	11.5	14.7	16.2	19.3	21.0	25.0	28.7	31.0	41.3	55.0	65.2	68.2	78.7	92.1

The results when observing the response of all microphone positions but with only one source at a time are compared. On one hand, source 1 is situated at the front right corner of the bus cabin at a low height. When observing the FRF measured with this source position almost all modes are excited, as can be observed in Figure 4.16. However, due to the large length of the bus, some modes are highly damped and difficult to observe only with this source position, especially above 70 Hz; and the mode at 55 Hz is not excited at all. The same effect occurs at source position 5, which is located also in a corner, although in this case the amplitudes of the modes are generally higher and the mode at 55 Hz appears, in contrast to position 1. These results can be further observed in Figure H.3 at Appendix H.

On the other hand, the rest of the sources are located at positions in the middle or the side of the bus, as seen previously in Figure 3.11. In these cases, the amplitudes of the modes are generally lower and some of the modes are not visible in the FRF. This is due to the location of these sources, which does not allow their excitation

as their placement corresponds to a location of low pressure levels. This can be observed in Figure 4.17 as an example, but it occurs also for sources 2 and 4 as shown in Figure H.2 and Figure H.2 respectively, at Appendix H.

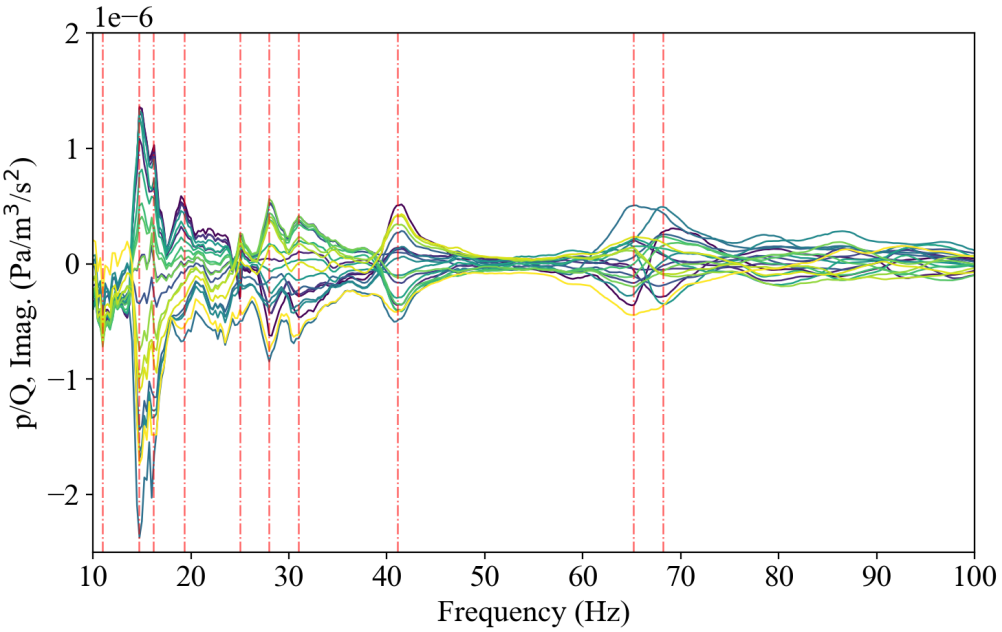

Figure 4.16: Imaginary part of the FRF measurement results for source 1, at the front right corner of the bus. The dash-dotted vertical red lines correspond to the higher resonant frequencies excited only with this source.

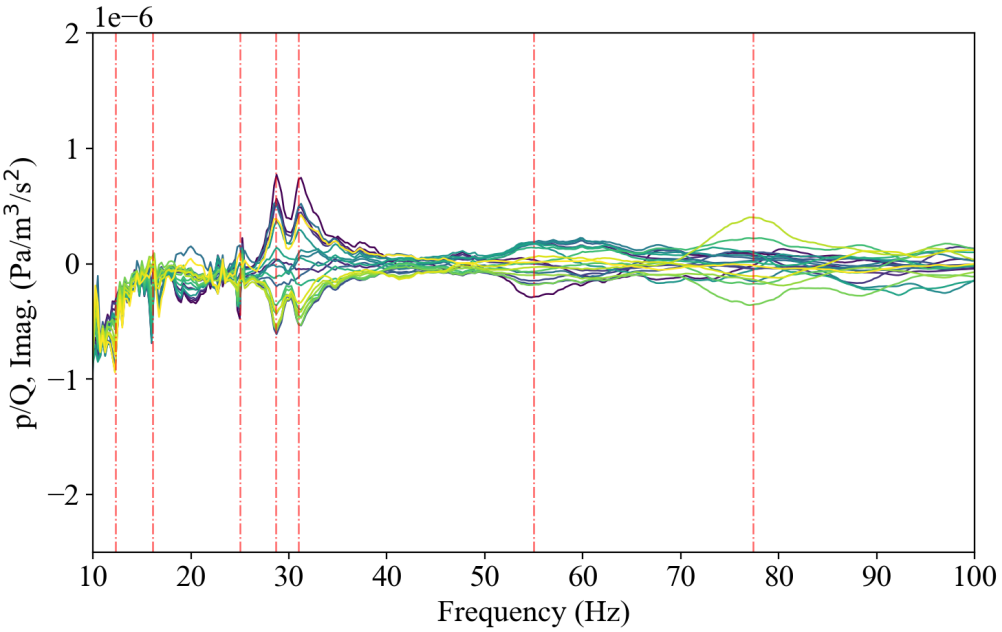

Figure 4.17: Imaginary part of the FRF measurement results for source 3, at the left side of the bus. The dash-dotted vertical red lines correspond to the higher resonant frequencies excited only with this source.

4.4 Comparison of Resonances

The correlation of the peaks presented previously for the simulation, SPL and FRF measurements is discussed in this section. In Table 4.5, a summary of the frequency peaks is presented, as well as possible causes of amplification of the modes in the bus cabin. The vibration results are not specified in this table since the measurement points were too few to draw any major conclusions regarding the effect of the structure on the noise levels in the cabin. A more detailed table specifying all the different driving cases for the SPL measurement and also the vibration results is to be found in Appendix I.

Firstly, some frequency peaks are visible only during the SPL measurements; these are shown in orange in the table. These are of course of importance for the passengers and can potentially cause annoyance. However, since they are not amplified by the cavity, but are rather due to noise from specific components active during operation, they are not included in the scope and will not be further discussed.

At frequencies up to 30 Hz there are not numerous modes in the bus model. In the frequencies where there are no theoretical modes in the cavity model but resonances in the FRF measurements occur, it can be assumed that the sound pressure peaks in the SPL results are due to structural modes. These modes are identified in yellow colour in the table. The structural modes can be further analysed, but this would require an extensive increase of vibration measurement points or a full impact test of the structure. The first peak in the SPL results has no response in the other methods, one reason for this being that the FRF measurement had a good response only above 10 Hz, which would not include this initial peak. Additionally, no cavity mode is present since the frequency is too low for a standing wave to occur in the longest direction of the bus. However, as discussed in Section 4.2.2, these frequencies are probably related to the rolling frequency of the tyres.

The most interesting frequencies and modes are those that have a peak in the results from all methods, displayed in green in the table. The peaks from the FRF measurement show that the frequency corresponds to an important mode. Additionally, the resonance in the SPL measurements indicates that the mode is excited while the bus is in operation. This means that it has an impact on the passenger and indicates how the sound field in the cabin is experienced.

Moreover, some frequencies were not proficiently excited with the FRF measurement; these are marked in blue in the table. What these peaks have in common is that they are above 70 Hz, which is where the modal density according to the simulation is increased remarkably. Looking at the mode shapes from the simulation, found in Appendix C, microphone and source positioning could be a reason for no clear modes appearing in the FRF results. For example, modes 7 – 10 in the simulation of the bus model have peaks at very low and very high heights in the bus. Therefore, the microphones, which were all placed at human ear heights, might not be sufficient to detect the peaks that should appear according to the simulation. However, this also indicates that these frequencies will not be the main cause of annoyance for the passengers.

Accordingly, mode 6 has a minimum and a maximum in the front of the bus, where two microphones, as well as a source position, were closely placed, leading to a mode that appears in the FRF measurements. Nevertheless, this analysis does not apply to all mode shapes, and it is also not representative to draw too harsh conclusions on the matter based on the visualisation from the simulations. This is because the pressure distribution inside the bus is not being shown, but only the pressure on the boundaries of the model. Simultaneously, the model is not an exact replica of the actual bus and factors such as damping, exact dimensions of the bus or material of the boundaries could potentially affect the peaks. Modal density in the frequencies over 70 Hz could also be a reason for it being hard to view clear peaks in the FRF results.

In summary, it has been shown that FRF measurements gave results correlating well with the simulation up until the frequency where the modal density increased. Some areas could be further studied to achieve a correlation between simulation and measurements in frequencies where the modal density is higher. The SPL measurements were an asset to determine whether the modes had an impact on the sound pressure levels that directly affect the passengers.

Table 4.5: Main resonances of the bus up to 100 Hz, obtained with three different methods: modal extraction simulation, FRF measurements and SPL measurements in operation.

Main resonances (Hz)			
Modal extraction	FRF measurement	SPL measurements	Resonance amplified by
		2.0 – 7.6	structure
	11.5	9.5 – 11.7	structure
14.4	14.7	13.4 – 14.9	cavity
	16.2	16.8 – 17.8	structure
	19.3	18.0 – 18.8	structure
	21.0	22.0 – 23.4	structure
26.5	25.0	26.1 – 26.8	cavity
	28.7	26.9 – 28.8	structure
	31.0	30.0 – 31.3	structure
		33.0 – 35.6	other
		36.1 – 39.8	other
41.3	41.3	40.7 – 41.9	cavity
		44.7 – 46.6	other
54.0	55.0	52.5 – 56.8	cavity
		56.6 – 62.0	other
64.0	65.2	64.5 – 65.2	cavity
68.9	68.2	67.6 – 69.8	cavity
70.8		70.1 – 70.3	cavity (not excited in FRF)
71.9		71.3	
72.3		72.0 – 72.3	
74.4		75.4	
76.3		75.9 – 77.6	
79.3	78.7	80.0	cavity
82.5		81.5	cavity (not excited in FRF)
87.2		87.4 – 88.4	
90.1		89.1	
91.3	92.1	90.8 – 91.0	cavity
95.0		93.3	cavity (not excited in FRF)
98.1		99.1	

5

Conclusion

The aim of this thesis was to compare the acoustic modal analysis of a bus cavity performed by FEM simulation and experimentally, by stationary FRF measurements and SPL measurements under operation. Consequently, the purpose was to identify the potential noise sources amplifying each resonance and the most important frequencies and positions of annoyance for passengers and drivers inside the cabin, as well as the adequacy of the methods. Based on the obtained results, it exists a good correlation between the modal extraction obtained with FEM analysis and both measurement methods, especially below 70 Hz. Above this frequency the high modal density and the variation in frequencies of excitation for the different test cases make it challenging to separate individual modes in the SPL results. Additionally, taking into account the large volume of the bus, the number of sources used in the FRF measurements may not be enough to excite the cavity modes at higher frequencies.

At low frequencies, which is the main interest of this thesis, the modelled bus can be considered accurate as the small parts inside the cabin have minimal impact on the cavity modes. However, as the bus was modelled with rigid boundaries, the modes obtained with the simulation correspond to pure cavity modes. Damping in the cabin and therefore the amplitude of the modes are not representative, but the simulation is really useful to have an idea of the resonance frequencies. On the contrary, in the case of the measurements, the structure and materials of the bus and the different noise sources influencing the interior sound field of the vehicle play an important role.

By performing both theoretical and experimental modal analyses it is possible to separate the pure cavity modes from those excited by the structure. To obtain these results only with simulations, a fully coupled fluid-structure model including all material properties would be necessary, which requires a more complex FEM analysis to obtain accurate and representative results. Because of this, to perform also experimental measurements is considered fundamental.

For future work, comprehensive measurements with a larger amount of microphone and source positions could be performed to obtain sufficient excitation of the modes in a broader frequency range. Isolation of individual components and extended vibration measurements could be also done in the SPL measurements to further analyse certain noise sources and therefore suggest improvements to improve the comfort of the passengers and drivers.

Bibliography

[1] World Health Organization (WHO). *Environmental and Health - Noise*. https://www.euro.who.int/en/health-topics/environment-and-health/noise. Accessed: 2022-03-16.

[2] G.M.L. Gladwell. "A finite element method for acoustics". In: *5th International Congress on Acoustics, Liège, Belgium* (Sept. 1965).

[3] D. Nefske and L.J. Howell. "Automobile interior noise reduction using finite element methods". In: *SAE Transactions* 87 (1978), pp. 1727–1737.

[4] G. Accardo et al. "Experimental Acoustic Modal Analysis of an Automotive Cabin". In: *SOUND VIBRATION* MAY (2015), pp. 10–18.

[5] H. Tsuji et al. "Experimental Method Extracting Dominant Acoustic Mode Shapes for Automotive Interior Acoustic Field Coupled with the Body Structure". In: *SAE International* (2013), pp. 1139–1146.

[6] *FACT SHEET Engine D5K240, EU6SCR*. https://stpi.it.volvo.com/STPIFiles/Volvo/FactSheet/D5K240,%20EU6SCR_Eng_01_1516474.pdf. Accessed: 2022-03-15.

[7] *FACT SHEET Gearbox AT2412E*. http://productinfo.vtc.volvo.se/STPIFiles/Volvo/FactSheet/AT2412E_Eng_03_1685344.pdf. Accessed: 2022-03-15.

[8] *Technical Introduction Volvo 7900 Electric Hybrid. Design and Function. Student Booklet GT2000783 Version 1*. Volvo Buses, Sept. 2016.

[9] T.E. Vigran. *Buildings Acoustics*. 2 Park Square, Milton Park, Abingdon, Oxon OX14 4RN: Taylor Francis, 2008, pp. 110–111.

[10] W. Desmet and P. Sas. *Numerical Acoustics Theoretical Manual*. LMS International.

[11] M. Petyt. *Finite Element Techniques for Acoustics*. Vienna: Springer, 1983.

[12] Free Field Technologies SA. *Actran 2021 User's Guide Vol.1*. Mont-Saint-Guibert: Free Field Technologies, 2020.

[13] N.M. Papadakis. "Application of Finite Element Method for Estimation of Acoustic Parameters". PhD thesis. Technical University of Crete, 2017.

[14] D. Nefske and L.J.Howell. "Six boundary elements per wavelength: Is that enough?" In: *Journal of Computational Acoustics* 10 (2002), pp. 25–51.

[15] ISO 16121-4:2011. *Road vehicles – Ergonomic requirements for the driver's workplace in line-service buses – Part 4: Cabin environment*. Standard. Geneva, Switzerland: International Organization for Standardization, Sept. 2011.

[16] G.-B. Stan, J.-J. Embrechts, and D. Archambeau. “Comparison of Different Impulse Response Measurement Techniques”. In: *Journal of the Audio Engineering Society* 50 (4 Apr. 2002).

[17] A. Farina. “Advancements in impulse response measurements by sine sweeps”. In: *Journal of the Audio Engineering Society* (May 2007).

[18] *Simcenter Qsources low frequency monopole source. Product Information.* `https://www.qsources.be/wp-content/uploads/2020/07/07-Siemens-SW-Simcenter-Qsources-Low-Frequency-Monopole-Source-Q-MED-PIS.pdf`. Accessed: 2022-04-28.

[19] ISO 5128:1980. *Acoustics — Measurement of noise inside motor vehicles.* Standard. Geneva, Switzerland: International Organization for Standardization, Aug. 1980.

[20] M. A. Sanderson and T. Onsay. “CAE Interior Cavity Model Validation using Acoustic Modal Analysis”. In: *SAE International* (2007).

[21] R.J. Bernhard, M. Moeller, and S. Young. *Automobile, Bus and Truck Interior Noise and Vibration Prediction and Control, in Handbook of Noise and Vibration Control.* Ed. by M.J. Crocker. John Wiley Sons, Inc., 2007, pp. 1159–1169.

A

Measurement Equipment

In this Appendix, tables with all used equipment for both SPL and FRF measurements respectively are shown. Additionally, a diagram of the FRF measurement chain is shown in Figure A.1.

Table A.1: Equipment list for SPL measurements.

Equipment	Brand	Type	Quantity
Triaxial accerelerometers	B&K	4506	2
Microphone + preamplifier	B&K	4189-A-021	8
Microphone calibrator	B&K	4231	1
PAK system	Müller-BBM	PAK mobile MK II	1

Table A.2: Equipment list for FRF measurements.

Equipment	Brand	Type	Quantity
Microphone + preamplifier	B&K	4189-A-021	20
Microphone calibrator	B&K	4231	1
Monopole source	Siemens	Q-MED	1
Electronic protection device	Siemens		1
Power amplifier	Siemens	LMS Q-AMP230V	1
Acquisition system	Siemens	Simcenter SCADAS	1

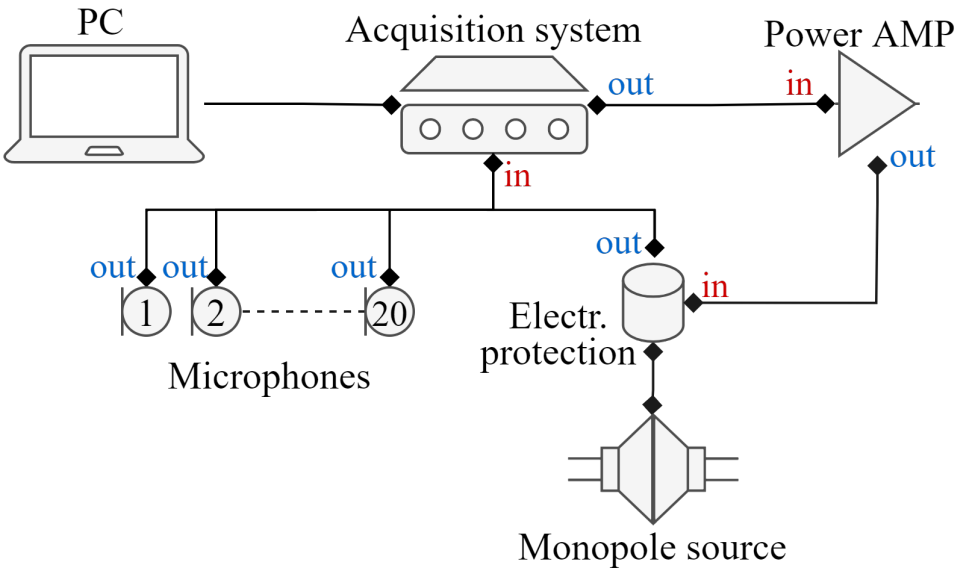

Figure A.1: FRF measurement chain.

B

Transducer Positions

This Appendix includes tables with the description of each transducer position. The pictures of the microphone positions used both in the SPL and FRF measurements and the accelerometer positions used to measure the vibration also in the SPL measurement, as well as of the source positions in the FRF measurements can also be found here.

Microphone positions

Figure B.1: Microphone position 1.

Figure B.2: Microphone position 2.

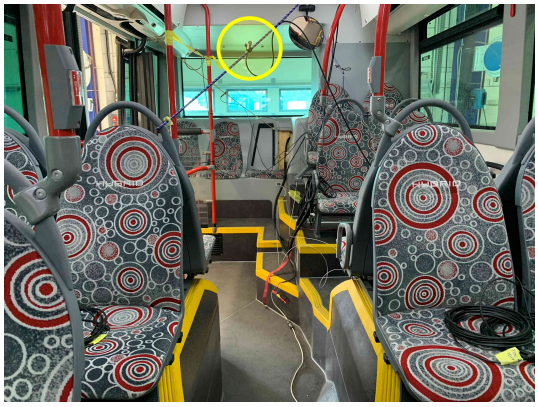

Figure B.3: Microphone position 3.

Figure B.4: Microphone position 4.

Table B.1: Description of microphone positions and heights for SPL and FRF measurements. The cells marked in grey correspond to heights measured above the seat cushion.

Measurement	Mic. position	Description	Passenger position	Height (m)
SPL and FRF	1	Rear Bench (middle)	seated	0.78
	2	Driveline	seated	0.72
	3	Rear axle	standing	1.52
	4	Rear door	standing	1.82
	5	Between axles	standing	1.6
	6	Mid door	standing	1.7
	7	Front axle	standing	1.44
	8	Drivers ear	seated	0.75
FRF	9	First row right	seated	0.70
	10	First row left	seated	0.80
	11	Four seats rear	seated	0.75
	12	Rear axle right	seated	0.70
	13	Rear axle left	seated	0.53
	14	Middle right	seated	0.52
	15	Middle left	seated	0.60
	16	Folding seat	seated	1.00
	17	Wheelchair	standing	1.50
	18	Four seats front	seated	0.88
	19	Backwards front	seated	0.60
	20	Front door	standing	1.73

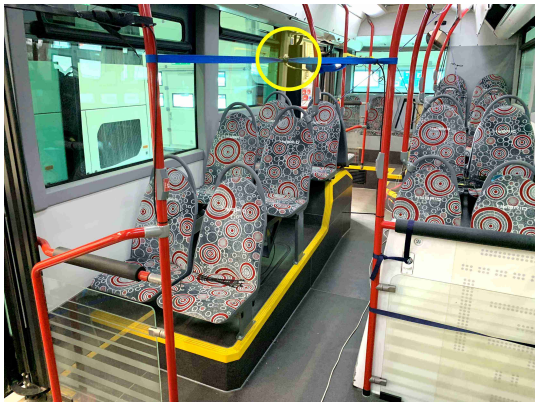

Figure B.5: Microphone position 5.

Figure B.6: Microphone position 6.

Figure B.7: Microphone position 7.

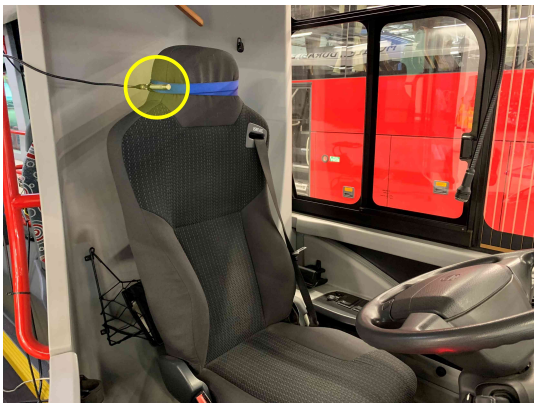

Figure B.8: Microphone position 8.

Figure B.9: Microphone position 9.

Figure B.10: Microphone position 10.

Figure B.11: Microphone position 11.

Figure B.12: Microphone position 12.

Figure B.13: Microphone position 13.

Figure B.14: Microphone position 14.

Figure B.15: Microphone position 15.

Figure B.16: Microphone position 16.

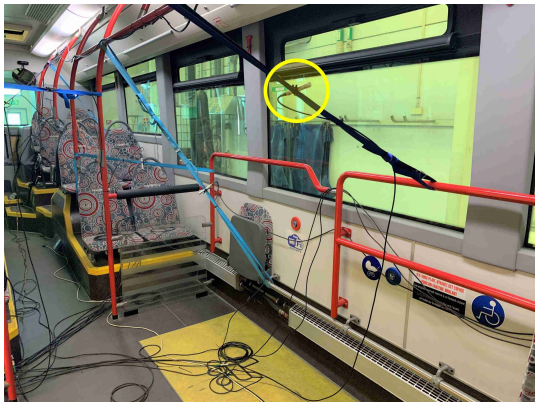

Figure B.17: Microphone position 17.

Figure B.18: Microphone position 18.

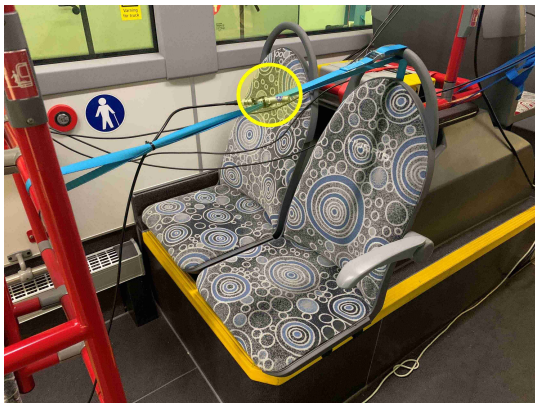

Figure B.19: Microphone position 19.

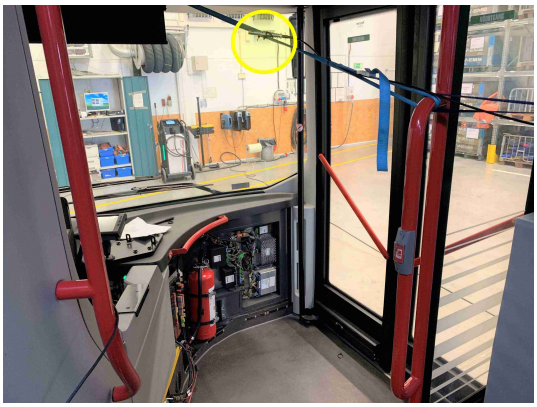

Figure B.20: Microphone position 20.

Accelerometer positions

Figure B.21: Vibration position 1: rear bench.

Figure B.22: Vibration position 2: driveline.

Source positions

Table B.2: Description of source positions and heights for FRF measurements.

Source position	Description	Height (m)	Distance to closest window (m)
1	Front right corner	0.75	0.5
2	Front axle	1.72	1.17
3	Left side	1.10	0.38
4	Rear axle	1.50	1.20
5	Corner rear panel	1.90	0.45

Figure B.23: FRF source position 1.

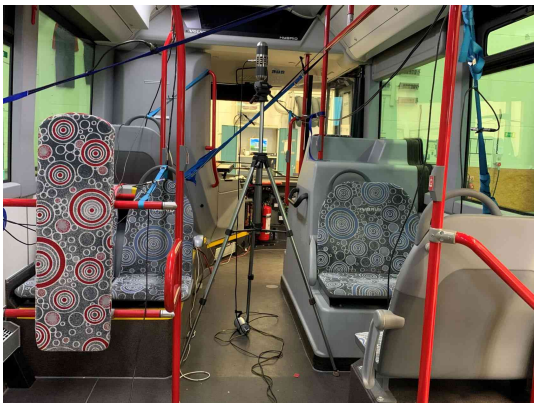

Figure B.24: FRF source position 2

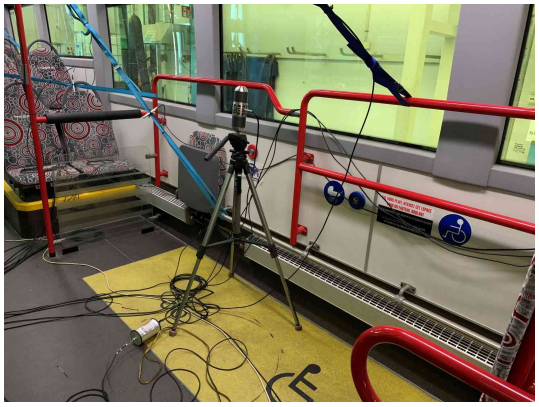

Figure B.25: FRF source position 3.

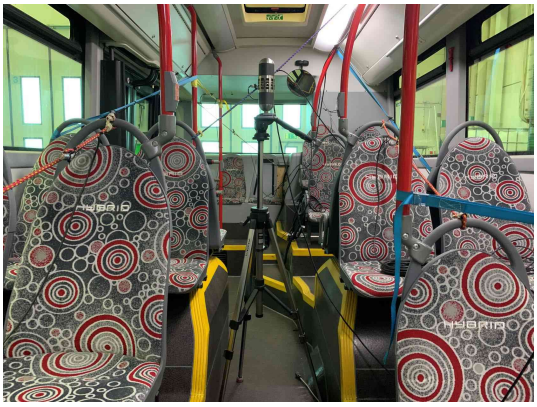

Figure B.26: FRF source position 4.

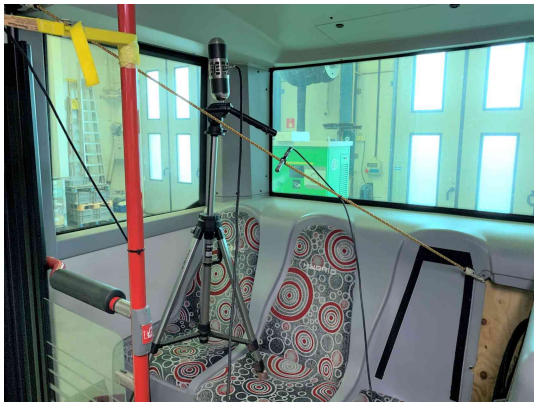

Figure B.27: FRF source position 5.

C

Modes in the FEM Models of the Rectangular Box and Bus Model

In this Appendix, the mode shapes, i.e. pressure distribution, for the 10 first modes are presented for both models made in Actran. The first ones are very alike, but they start to differ with the increased frequency.

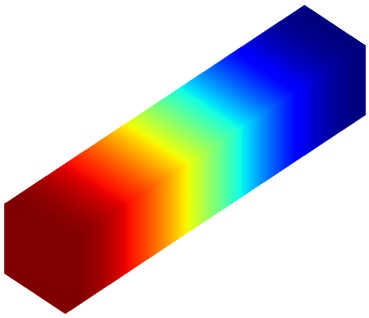

Figure C.1: Box model mode 1, f = 14.41 Hz.

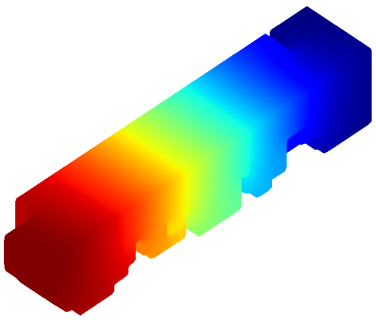

Figure C.2: Bus model mode 1, f = 14.47 Hz.

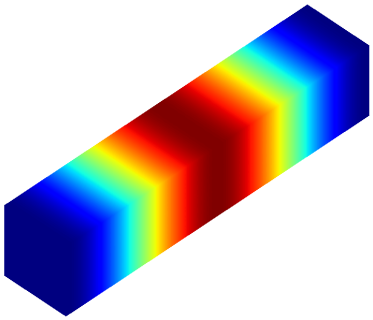

Figure C.3: Box model mode 2, f = 28.82 Hz.

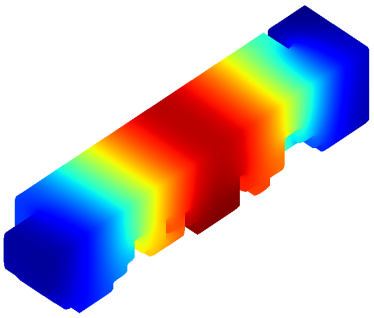

Figure C.4: Bus model mode 2, f = 26.50 Hz.

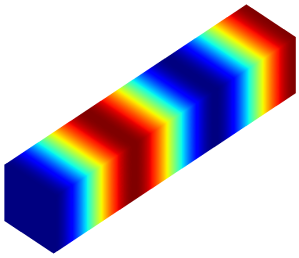

Figure C.5: Box model mode 3, f = 43.23 Hz.

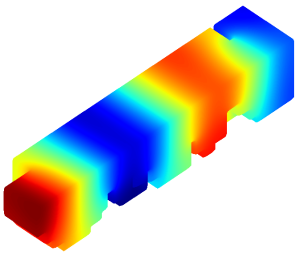

Figure C.6: Bus model mode 3, f = 41.30 Hz.

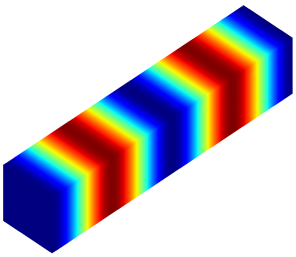

Figure C.7: Box model mode 4, f = 57.65 Hz.

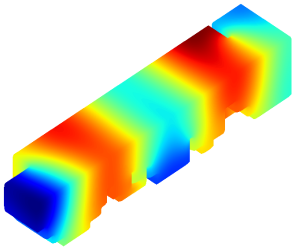

Figure C.8: Bus model mode 4, f = 54.10 Hz.

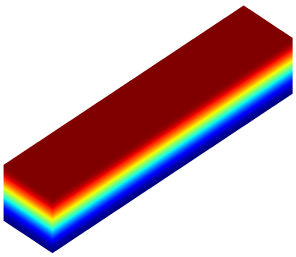

Figure C.9: Box model mode 5, f = 66.18 Hz.

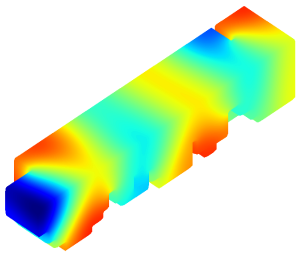

Figure C.10: Bus model mode 5, f = 63.91 Hz.

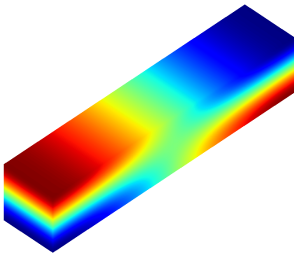

Figure C.11: Box model mode 6, f = 67.73 Hz.

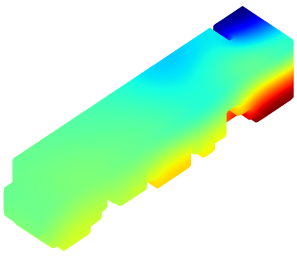

Figure C.12: Bus model mode 6, f = 68.85 Hz.

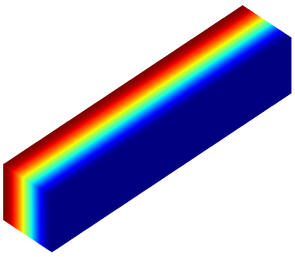

Figure C.13: Box model mode 7, f = 70.58Hz

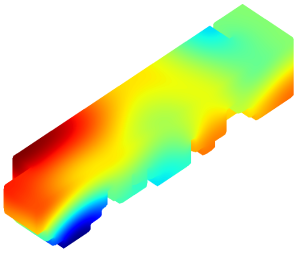

Figure C.14: Bus model mode 7, f = 70.78 Hz.

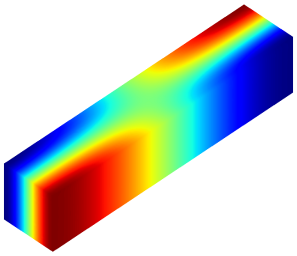

Figure C.15: Box model mode 8, f = 72.04 Hz.

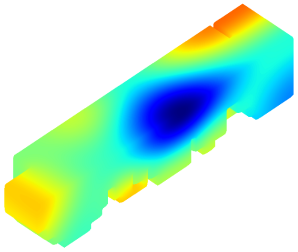

Figure C.16: Bus model mode 8, f = 71.83 Hz.

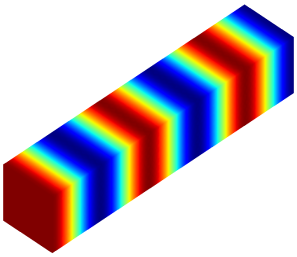

Figure C.17: Box model mode 9, f = 72.08 Hz.

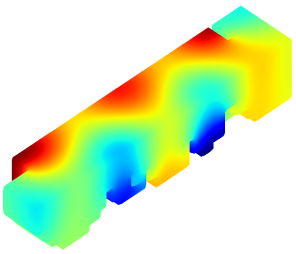

Figure C.18: Bus model mode 9, f = 72.18 Hz.

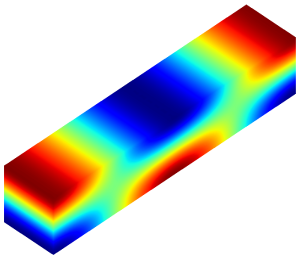

Figure C.19: Box model mode 10, f = 72.20 Hz.

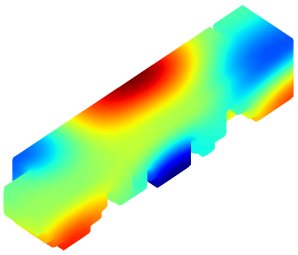

Figure C.20: Bus model mode 10, f = 74.38 Hz.

D

Frequency Response of the Bus Model

The frequency response results obtained with the simulation are shown in this Appendix for the different sources independently. All the resonant peaks are visible in all the plots for the different source positions. Above 65 Hz the amplitude of the resonant peaks slightly differs between the different plots.

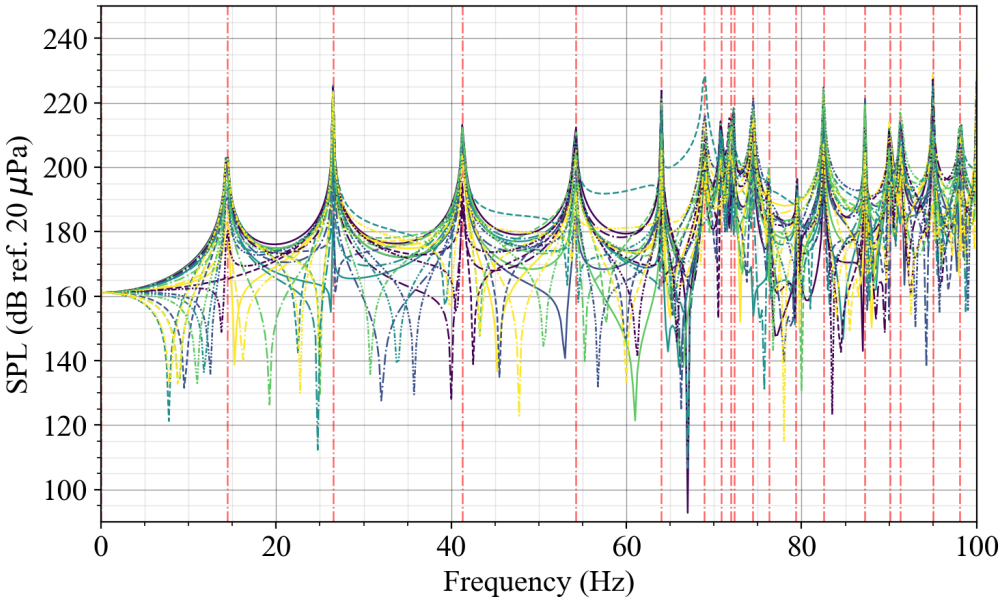

Figure D.1: Frequency response in the bus model with source 1 at the corner activated.

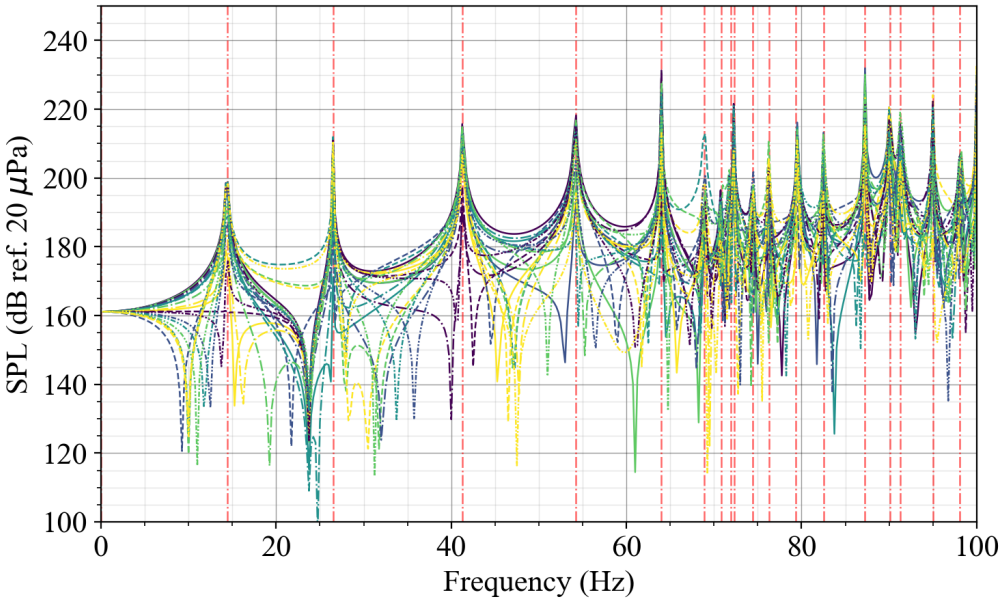

Figure D.2: Frequency response in the bus model with source 2 at the front axle activated.

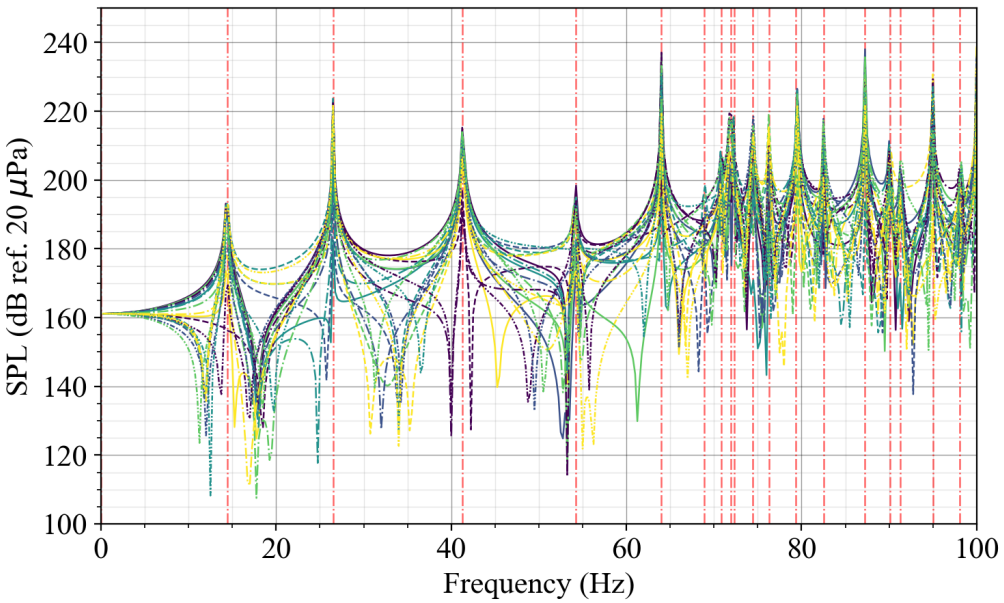

Figure D.3: Frequency response in the bus model with source 3 at the left side activated.

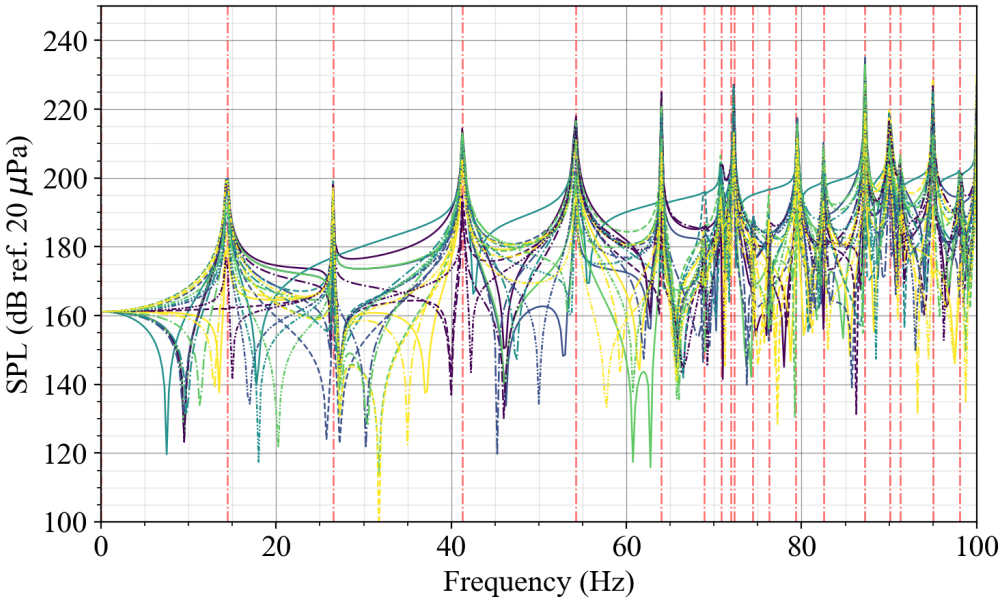

Figure D.4: Frequency response in the bus model with source 4 at the rear axle activated.

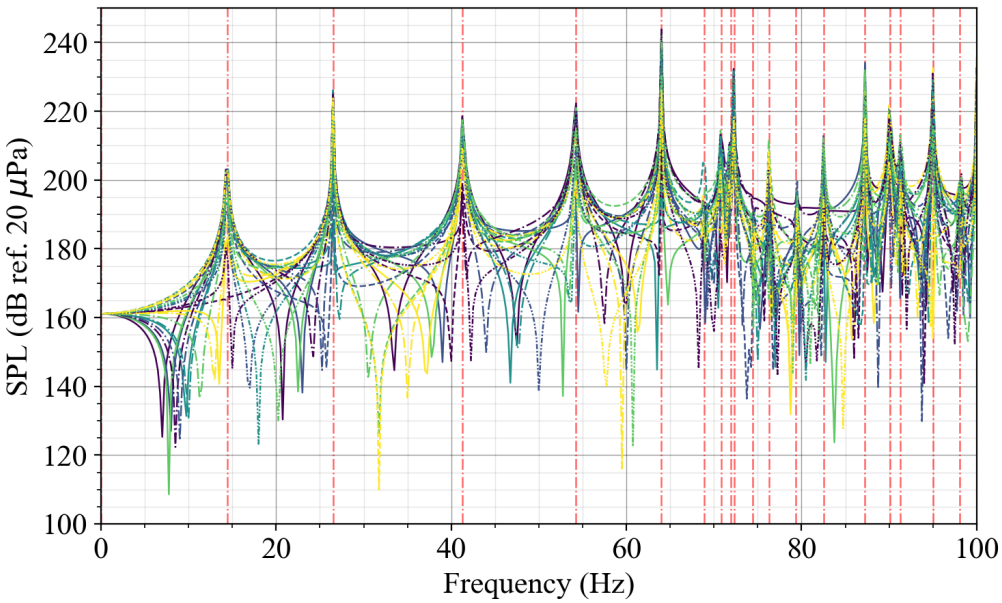

Figure D.5: Frequency response in the bus model with source 5 at the rear panel activated.

E

FFT Results from SPL Measurements

The results of the FFT performed on the SPL measurements are shown in this Appendix for the different test cases in the frequency range 0 Hz – 100 Hz.

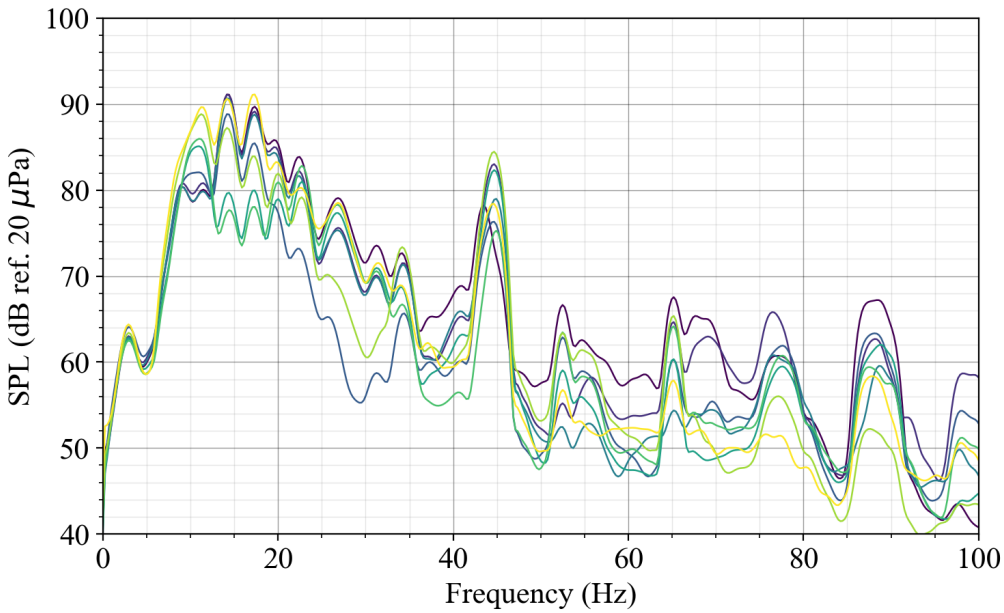

Figure E.1: FFT for 30 km/h and all microphone positions.

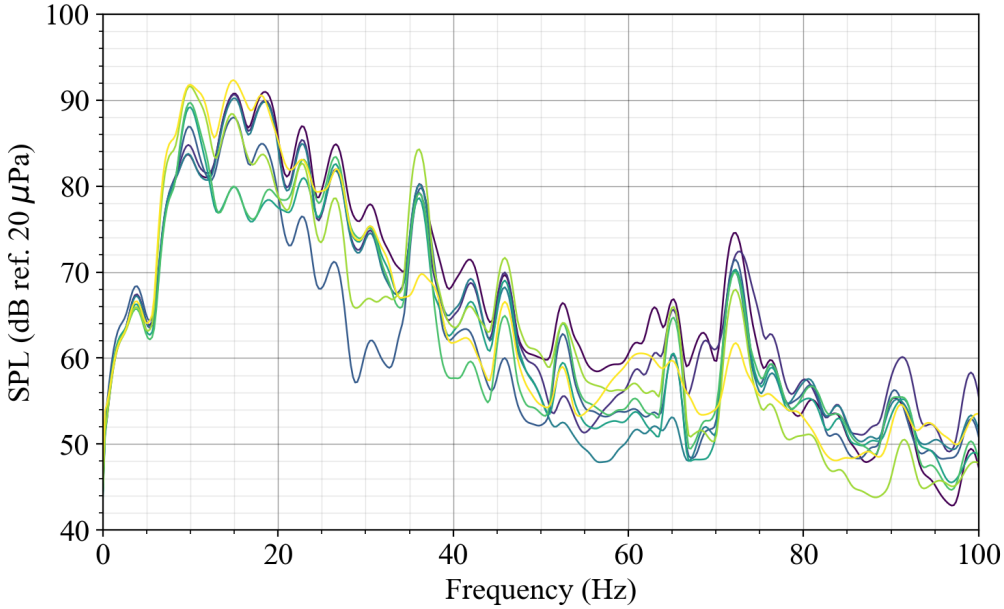

Figure E.2: FFT for 40 km/h and all microphone positions.

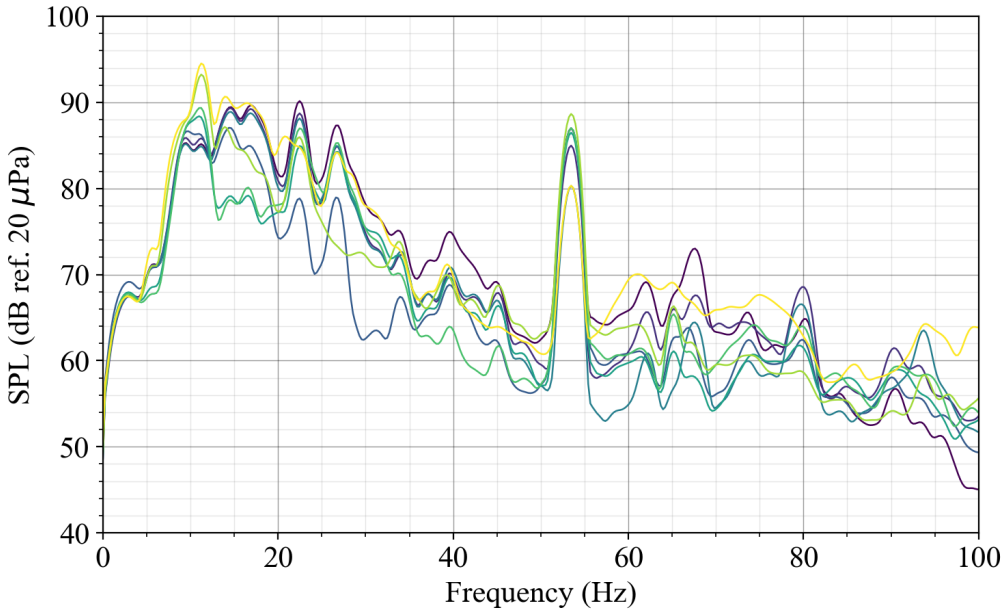

Figure E.3: FFT for 60 km/h and all microphone positions.

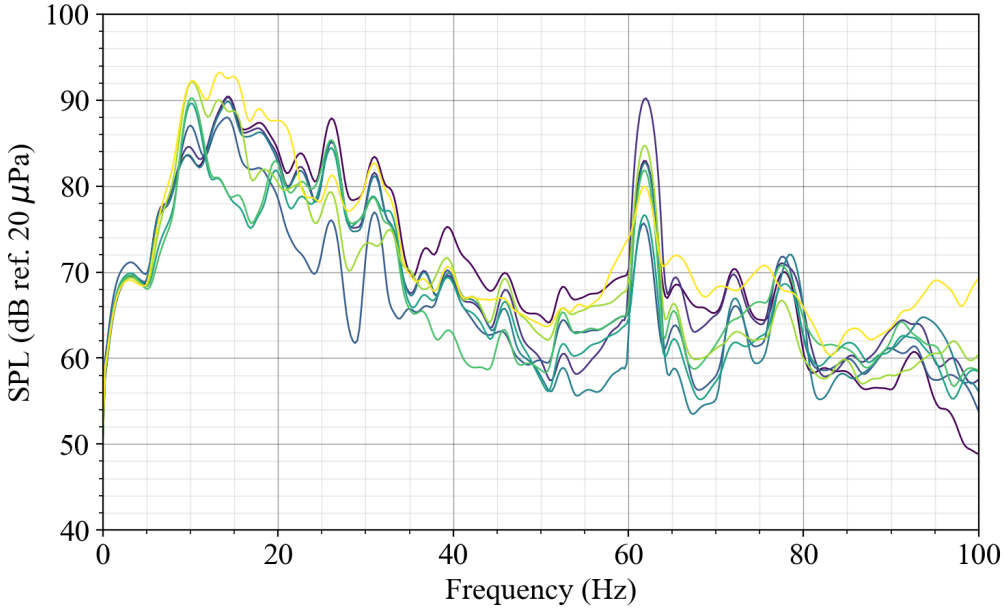

Figure E.4: FFT for 70 km/h and all microphone positions.

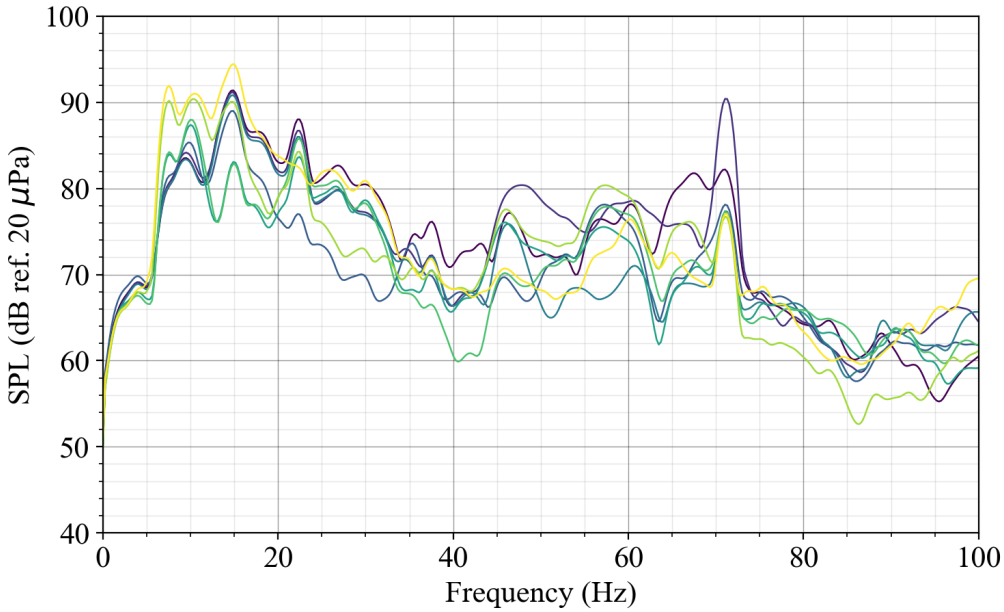

Figure E.5: FFT for the WOT test case and all microphone positions.

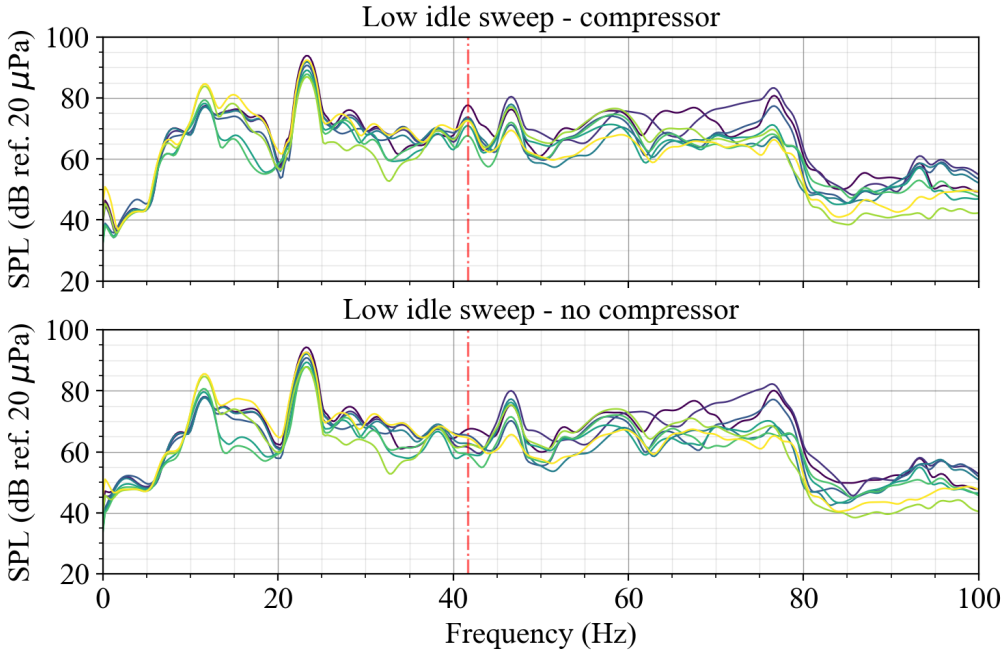

Figure E.6: FFT for the low idle sweep test case with compressor (upper) and without compressor (lower) for all microphone positions. The dash-dotted vertical red lines correspond to the resonance which presents the most evident variation between both test cases.

F

Rotational Speed of the Wheel

The rotational speed of the wheel can excite the vehicle and have an impact on the noise levels in the cabin. A theoretical investigation of in what range the tires might have an effect has been done and how the calculation was performed is described in this Appendix.

The wheels on the bus used during SPL measurements had a tyre width of 275 mm, the diameter of the wheel is 22.5 in and the aspect ratio is 70 %. The total wheel and tire diameter is calculated as

$$\text{rotational speed of wheel} = \text{vehicle speed} \cdot c \tag{F.1}$$

where the vehicle speed shall be in m/min and circumference (c) in m to get the rotational speed in RPM, 1/min. Since the dimensions specified on the tyre do not include the diameter of the total tire and wheel it has to be calculated from the aspect ratio. The sidewall height of the tyre is

$$h = \text{wheel width} \cdot \text{aspect ratio} = \frac{10.8 \text{ in}}{0.0254} \cdot 0.70 = 0.19 \text{ m}, \tag{F.2}$$

where the division is to convert it from inch to meter. This is then added to the wheel diameter, which results in a diameter of 0.957 m.

The circumference of the wheel is calculated as

$$c = \text{tire diameter} \cdot \pi = 0.19 \text{ m} \cdot \pi = 3.1 \text{ m}. \tag{F.3}$$

The theoretical rotational speed of the wheel and tyres for the different constant speeds is presented in Table F.1 and it is shown that the tyres could excite the modes at very low frequencies.

Table F.1: Resonant frequencies detected in the FRF curves in the range 10 Hz-100 Hz for all sources.

Peak	20	30	40	50	60	70	80
Freq. (Hz)	1.85	2.77	3.70	4.62	5.55	6.47	7.5

G

FFT and Order Analysis for Rollout Cases

The rollout in *Drive* mode (D), shown in Figure G.1, has a clear second order but other than that not much of significance. The gear changes are visible in Figure 4.13 since they can be directly correlated with the RPM of the engine.

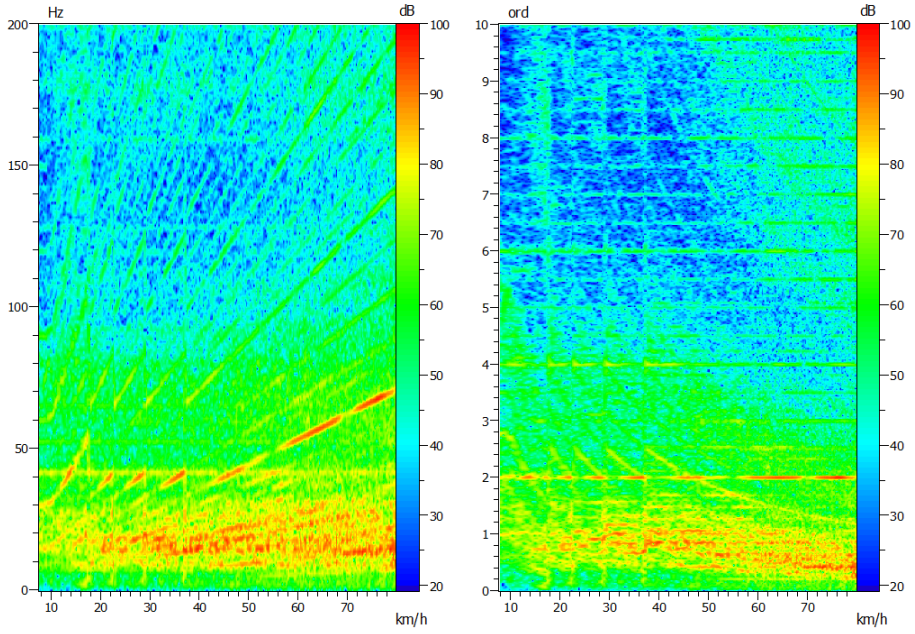

Figure G.1: FFT over vehicle speed (left) and Order analysis (right) for Rollout in D at rear bench.

The vehicle retard slower in *Neutral* (N) made it necessary to measure on both straights of the test track, therefore it is presented in two different figures, Figure G.2 and Figure G.3. The first rollout from 80 km/h has clear second and fourth orders but also some higher harmonics as well. The dominant frequencies are around 24 Hz as well as around 47 Hz. The second rollout from 60 km/h in Figure G.3 also has some harmonic components in the left graph at: 23 Hz, 48 Hz, 70 Hz, 93 Hz, 116 Hz and 140 Hz.

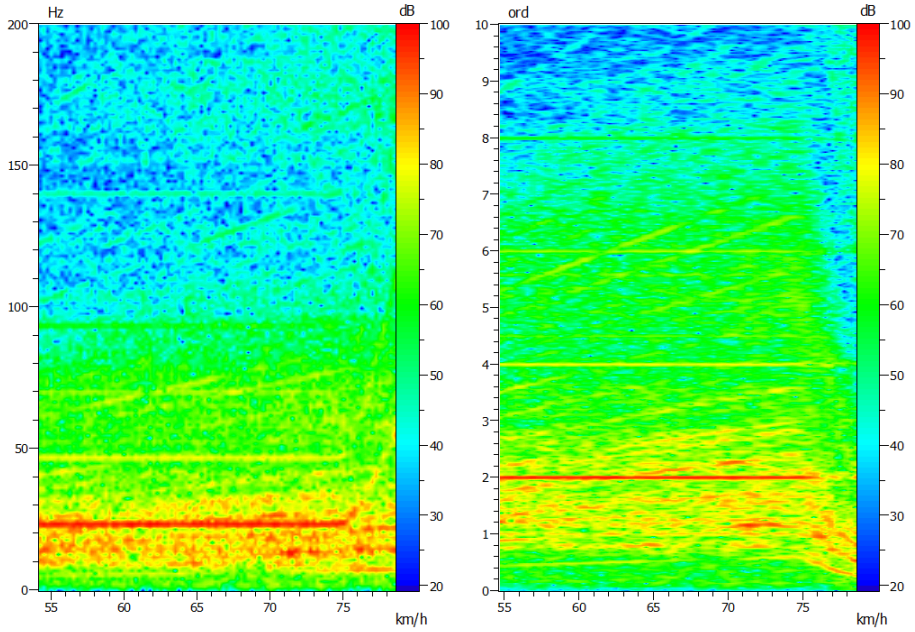

Figure G.2: FFT over vehicle speed (left) and Order analysis (right) for Rollout in N from 80 km/h at rear bench.

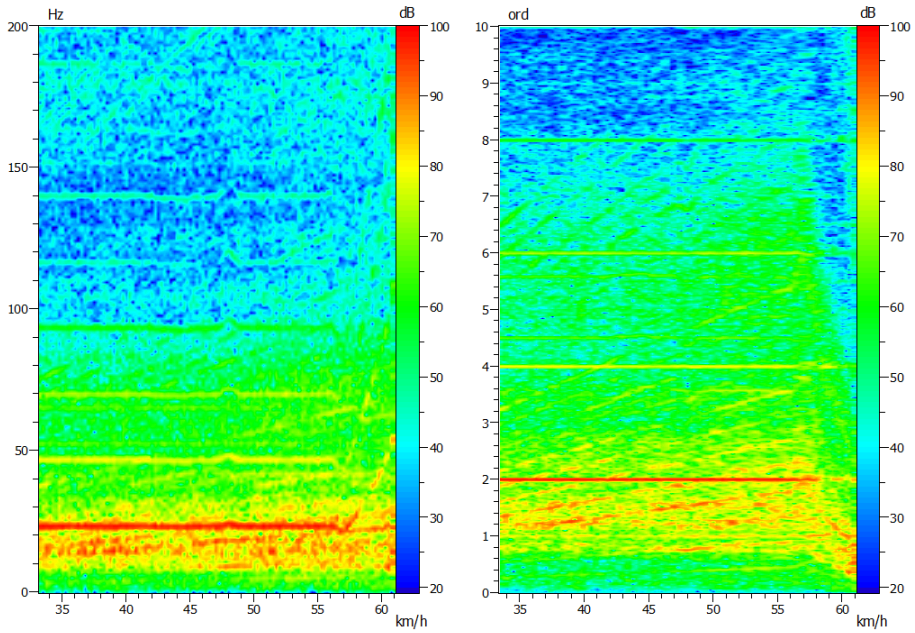

Figure G.3: FFT over vehicle speed (left) and Order analysis (right) for Rollout in N from 60 km/h at rear bench.

H

FRF Additional Results

The FRF results from the measurements are shown in this Appendix for a larger frequency range than those presented in the report. The plots for the FRF of sources 2, 4 and 5 independently are found here as well. Lastly, for source 4, the same results are presented both in imaginary part (Figure H.4) and magnitude (Figure H.5) for comparison purposes.

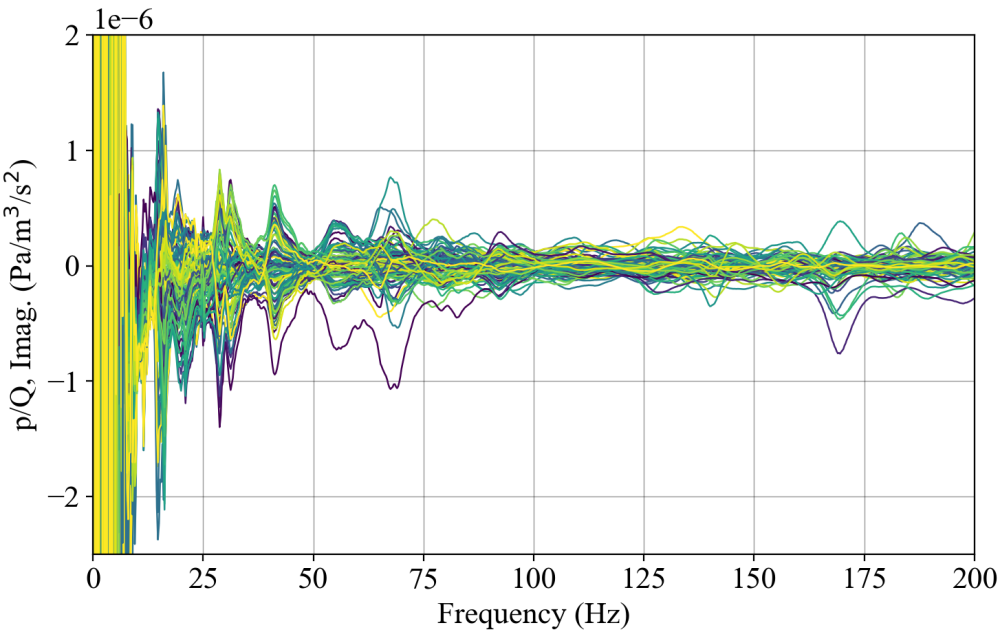

Figure H.1: Imaginary part of the FRF measurement results for all sources between 0 Hz and 200 Hz.

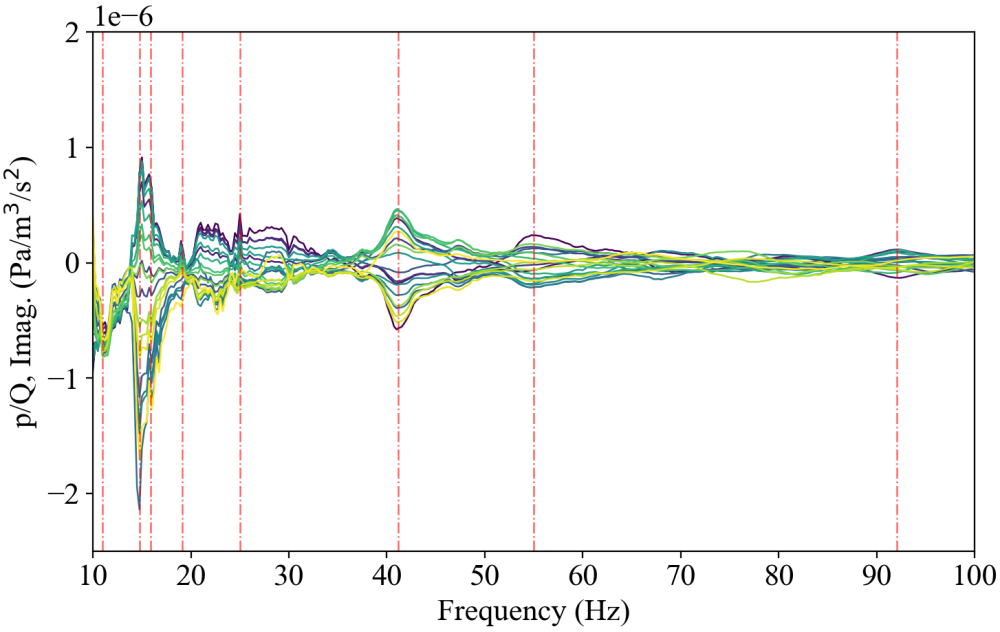

Figure H.2: Imaginary part of the FRF measurement results for source 2. The dash-dotted vertical red lines correspond to the higher resonant frequencies excited only with this source.

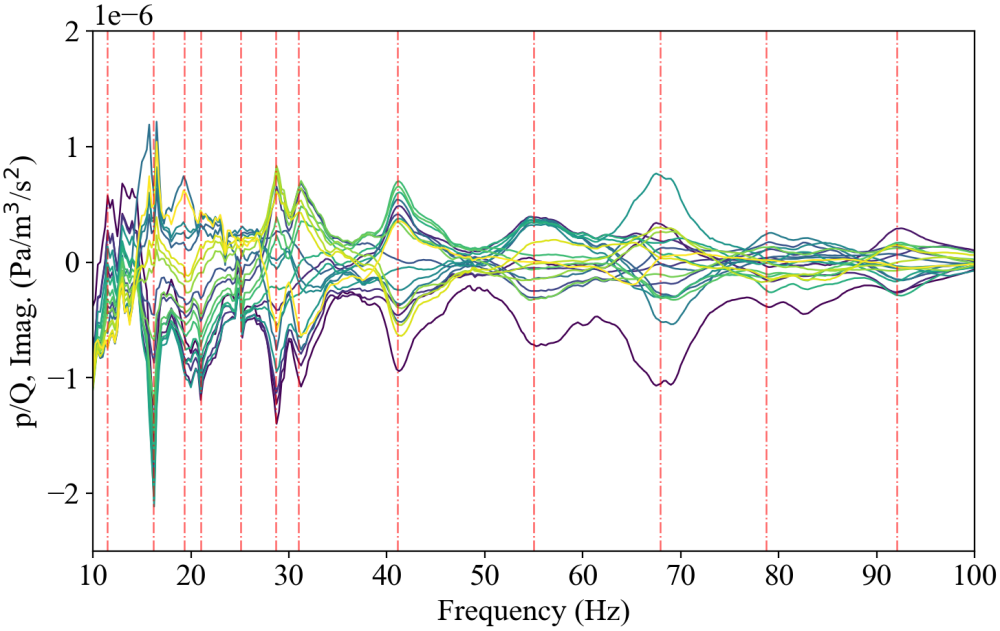

Figure H.3: Imaginary part of the FRF measurement results for source 5. The dash-dotted vertical red lines correspond to the higher resonant frequencies excited only with this source.

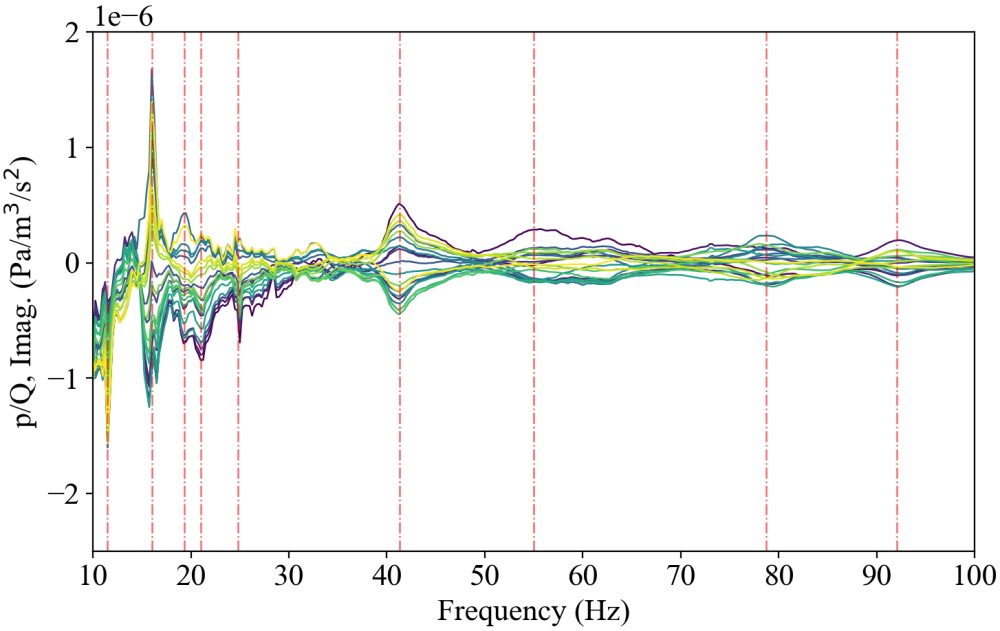

Figure H.4: Imaginary part of the FRF measurement results for source 4. The dash-dotted vertical red lines correspond to the higher resonant frequencies excited only with this source.

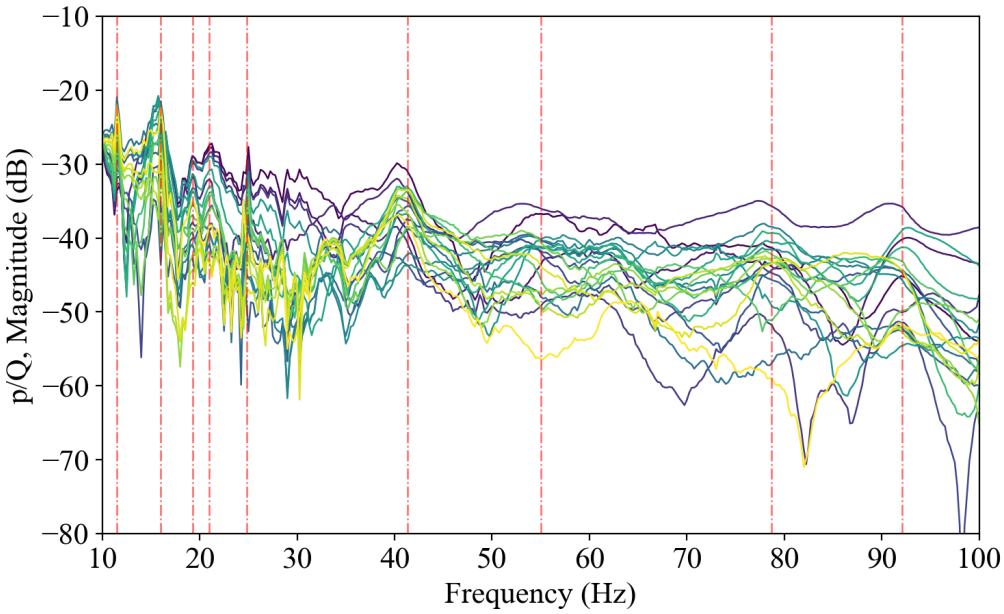

Figure H.5: Magnitude in dB of the FRF measurement results for source 4. The dash-dotted vertical red lines correspond to the higher resonant frequencies excited only with this source.

I

Summary of All Resonance Peaks

The resonance peaks found in the results from the SPL, FRF and simulation plots are presented in the two following tables: Table I.2 and Table I.3. The colours of the cells in the tables are an indication of whether it is a clear peak or not for the SPL. For the FRF and simulation results, which have 5 results (one for each source position), the darker colour shows if the peaks are visible for all source positions. The results of the vibration measurement, performed simultaneously as the SPL, are marked with a red number; if the cell does not have a background colour the peaks were only visible in the vibration measurements. The explanations are visibly explained in Table I.1.

Table I.1: Explanation of the colors used in Table I.2

Low peak
High peak
Peak in vibration results
Peak in vibration and SPL results
Peak in results for all source positions
Low peak for some of the source positions

Table I.2: All resonance peaks from measurements and simulation results below 60 Hz.

Resonance peaks below 100 Hz																
SPL and vibration measurements	Contant speed	20 km/h	2.0	9.7	13.4		18.5	22.9		27.1			**37.6**			52.5	
		30 km/h	2.9	11.2	14.2	17.3		22.5		26.9	31.3	34.2			**44.7**	52.5	
		40 km/h	3.9	10.0	14.9		18.5	22.7	26.6		30.5		**36.1**	41.9	45.9	52.5	
		50 km/h	4.6	9.5	14.4		18.8	22.7		28.3		33.0	37.8		**45.2**	52.5	56.6
		60 km/h	5.4	**11.2**	14.4	16.8		22.5	26.6			33.9	39.3			**53.5**	
		70 km/h	6.6	10.2	**14.4**	17.8		22.5	26.1		**31.0**		39.3		45.9		**62.0**
		80 km/h	**7.6**	10.7	**14.6**		18.0	22.5	26.1		30.0	**35.6**				53.2	
	WOT		**7.6**	10.5	**14.6**	17.8		22.5	26.8		30.0		37.6		**46.4**	**56.6**	60.3
	Low idle	compressor	7.1	11.7		17.6		**23.2**		28.8		34.9		41.7	**46.6**	52.5	58.1
		no compressor	7.1	11.7		17.6		**23.2**		28.8		34.9		40.7	**46.6**	52.5	58.1
	Low idle sweep	compressor		11.7	14.9	17.8		**23.2**		28.1	31.2	34.4	38.1	41.7	**46.6**		**58.1**
		no compressor		11.7		17.1		**23.2**		28.1	31.2	34.4	38.1	41.7	**46.6**		**58.1**
	Roll-out D	A (80-7 km/h)		10.0	**14.1**		18.0	22.0			30.1	34.0	39.8			56.8	59.0
		B (80-12 km/h)		9.8	**14.1**		18.0			27.3			38.8	41.5	**45.1**	**56.8**	59.6
	Roll-out N	A (80-54 km/h)		10.7	**13.9**		18.8	**23.4**	26.6		30.5				**46.6**	**56.6**	
		B (80-51 km/h)	7.3	**11.5**	13.9	17.8		**23.2**	26.8						**46.6**	**56.6**	
		A (60-33 km/h)		10.3	**14.2**		18.1	**23.4**							**46.6**		
		B (60-29 km/h)		10.9	**14.4**		18.6	**23.4**							**46.6**	**53.7**	
	MIN		7.1	9.5	13.4	16.8	18.0	22.0	26.1	26.9	30.0	33.0	36.1	40.7	44.7	52.5	56.6
	MAX		7.6	11.7	14.9	17.8	18.8	23.4	26.8	28.8	31.3	35.6	39.8	41.9	46.6	56.8	62.0
FRF measurement				11.5	14.7	16.2	19.3	21.0	25.0	28.7	31.0			41.3		55.0	
Modal extraction					14.4				26.5					41.3		54.2	

Table I.3: All resonance peaks from measurements and simulation results from 60 Hz to 100 Hz.

Resonance peaks below 100 Hz															
SPL and vibration measurements	Contant speed	20 km/h	65.2					**75.4**								
		30 km/h	65.2						76.4			**88.4**				
		40 km/h	65.2				**72.3**							91.0		
		50 km/h	65.2											**90.8**		
		60 km/h		67.6						80.0						
		70 km/h					72.0		77.6							
		80 km/h				**71.3**							**89.1**			
	WOT			67.6		**71.3**										
	Low idle	compressor	64.9	**69.8**					75.9		81.5	87.4			93.3	99.1
		no compressor	64.9	**69.8**					75.9		81.5	87.4			93.3	99.1
	Low idle sweep	compressor	64.5		**70.3**				**76.6**							
		no compressor	**64.5**						**76.6**							
	Roll-out D	A (80-7 km/h)		67.6	**70.3**											
		B (80-12 km/h)		**67.9**	**70.3**											
	Roll-out N	A (80-54 km/h)			**70.1**											
		B (80-51 km/h)			70.1											
		A (60-33 km/h)			**70.1**											
		B (60-29 km/h)			70.1											
	MIN		64.5	67.6	70.1	71.3	72.0	75.4	75.9	80.0	81.5	87.4	89.1	90.8	93.3	99.1
	MAX		65.2	69.8	70.3		72.3		77.6			88.4		91.0		
FRF measurement			65.2	68.2						78.7				92.1		
Modal extraction			64.0	68.9	70.8	71.9	72.3	74.4	76.3	79.3	82.5	87.2	90.1	91.3	95.0	98.1

Department of Architecture and Civil Engineering, Division of Applied Acoustics
CHALMERS UNIVERSITY OF TECHNOLOGY
Gothenburg, Sweden
www.chalmers.se

CHALMERS
UNIVERSITY OF TECHNOLOGY